RESEARCH STUDY: REACTING METAL BIS(TRIMETHYL)AMIDES WITH DOUBLE-BASE PROPELLANT STABILIZERS IN PURSUIT OF NOVEL PROPELLANT ADDITIVES

A Thesis
Submitted to
the Temple University Graduate Board

In Partial Fulfillment
of the Requirements for the Degree of
MASTERS OF ARTS, CHEMISTRY

---

by
Carl E. Lundell
May 2017

Thesis Approval:

Dr. Michael Zdilla, Thesis Advisor, Chemistry Department

ABSTRACT

During World War II, it was discovered that when lead was added to double-base propellants, it produced beneficial burn rate phenomena. Specifically, the propellant burn rate first increased unexpectedly at low pressures, then the burn rate became independent of pressure, followed lastly by "mesa burning" where the burn rate actually decreased with increasing pressure. This results in a beneficial negative feedback mechanism. Over the past 75 years, researchers have explored different lead complexes to achieve better propellant performance. However, over the last decade, research has shifted to finding an alternative to using lead as an additive to reduce toxicity. Until the attempts detailed herein, researchers had not, to our knowledge attempted to combine double-base propellant stabilizers with various metals to achieve these desired results. In doing so, we prepared two lead complexes, Tetrakis (μ_3-(4-methyl-3-nitrophenyl imido lead (II))) **1**, and Bis(dinitrophenyl imido lead(II)) **2**, that were synthesized by reacting lead bis(trimethylsilyl)amide with a common double-base propellant stabilizer 2-nitrodiphenylamine (NDPA) and 4-methyl-3-nitroaniline. Both complexes formed from protolysis of the trimethylsilylamide ligand by the acidic proton of the amine, and crystalized from tetrahydrofuran (THF). Bomb calorimetry coupled with crystal density structure determined that **1** has a very high energy density of 74.1 MJ/L, more than three times the energy density of conventional nitroamine explosives, whereas **2** was lower at 38.2 MJ/L. The structure, charge and characterization of **1** and **2** are discussed. However, each complex is air sensitive making burn rate experimentation infeasible, so any possible changes to the propellant as an additive remained undetermined. Attempts to

use of tin, zinc, or bismuth bis(trimethyl)amides in place of lead, were unsuccessfully characterized, although reactions were likely observed.

DEDICATION

This thesis is dedicated to my mother, Carole Lundell who always provided me the push required to achieve and do what others thought not possible. To my deceased father whom I know would be proud of my accomplishments. This is also dedicated to the numerous Soldiers, peers, and superiors that I have had the honor and pleasure of working with over my Army career.

ACKNOWLEDGMENTS

I express heartfelt thanks, and sincere appreciation to my research advisor Dr. Michael Zdilla. Being in a career that emphasizes leadership, Dr. Zdilla shirks academia stereotypes and displays leadership qualities the military tries to instill in its leaders. He foremost and importantly does not micromanage his research team and gave me free rein to make my own mistakes and learn to work in the lab at my own pace. He also provided valuable supervision, patience, and scholarly enlightenment that was necessary in completing my graduate studies. He always made time for me and other research members and made working in his lab a truly enjoyable experience. Thanks for giving me the opportunity to conduct research in your lab.

I also wanted to give a special thanks to other members of my research team, specifically the other upper graduate student, Mike Gau, and Owen O'Sullivan. Going back to school after 17 years involved a heathy learning curve in the lab and they were there to help me at every turn. Their contributions to my education could not be understated: they helped show me how to operate the glove box, use the IR, use the X-ray diffractometer, help me with research ideas and provide constant advice on a whole host of topics. You are all talented individuals and hope that you achieve whatever you strive for.

Finally, I thank my wife, Lisa and good friends Taylor Keller and Megan Van Vliet. It has been a great two years.

PREFACE

Chapter 1 is the introduction and is used to familiarize the reader with double-base propellants, and the importance of a burn rate phenomena associated with them. The chemistry reactions associated with double-base propellant combustion are also discussed. A research gap is identified and resulting research question is proposed.

Chapter 2 is a literature review and provides a scientific review of previous efforts to improve ballistic modifiers and double-base propellant stabilizers. A methodology to answer the research question is provided.

In chapter 3, the results of the successful crystallization of two lead complexes is discussed, as well as attempts using different metals. Each lead product is discussed in depth and their significance.

Chapter 4 is the conclusion. What the experiments answered, what questions remain unanswered, and what future research is required to fully answer the research question is discussed.

Chapter 5, the final chapter, is the experimental section of the manuscript.

TABLE OF CONTENTS

LIST OF FIGURES

Figure Page

LIST OF EQUATIONS

CHAPTER 1

INTRODUCTION: PROPELLANTS AND BURN RATE PHENOMENA

1.1 Propellants

1.1.1 Types of Propellants

Chemical propellants had their first recorded use in China in 1232, and will continue to be the primary propulsion system for rockets and missiles far into the future.[1] The use of nuclear power and other forms of energy remain in the infant stages and may play a substantial role in future space travel, for example, but will not compete with typical chemical propellants for decades or more to come. In fact, the conversion of chemical reactants into high temperature gases far exceed other propulsion systems such as jet engines. At the most basic level, propellants are composed primarily of two things: an oxidizer and fuel. Although some propellants have an oxidizer incorporated into the fuel, some have a separate oxidizer component. Chemical bonds are broken within the fuel and conditions are created for the chemical molecules to reform – the exothermic energy difference between bond energies broken and those reformed creates heat. As heat is created with gaseous products, in a confined space, high pressure is created that is focused into thrust through a nozzle.

Since their initial invention, chemical propellants have had numerous components added and upgraded, each for a specific purpose. The basic properties of propellants have changed a lot since their first use in China centuries ago, and three primarily diverse types have been developed: solid, liquid and hybrid.[1]

Solid propellants were the first propellants developed and saw almost exclusive use until recently, but retain many advantages over more modern types. Solid propellants have uncomplicated design and construction – making them cheaper, easier to maintain and more reliable. They also have a high density making them smaller and more compact than other types. However, they tend to be sensitive to temperature, unable to be restarted once stopped and require a shaping of the propellant grain to create thrust. Different geometric grain shapes, produce different burn rates. Another disadvantage is that solid propellants are intolerant of cracks or voids, so need to be rigorously checked for them (typically by X-ray) during production. The presence of voids within the propellant is from trapped air pockets that at a minimum, decrease rocket performance from the loss of propellant density. However, more concerning is the air creating 'worm holes' whereby the burning surface of the propellant is greatly increased over a short amount of time and results in over pressurization of the rocket motor and explosion. It is the rate that combustion moves through the propellant and the rate the fuel is consumed that dictates performance.[1] Solid propellants are extensively used in military missiles such as the, AGM-114 Hellfire, AIM-9E Sidewinder and Tomahawk cruise missiles (Figure 1). Solid propellants are also further subdivided into different types: single, double-base, triple-base, and composite. A common type, the double-base (DB) propellant, will be discussed at length later in the chapter.

Liquid propellants were developed after World War I, and have primarily two advantages over their solid counterparts. First, once combustion is started it can be stopped and restarted, and secondly - it typically produces more thrust than comparable solid propellant. However, liquid propellants require a more complicated system and are more subject to failure. This is because special attention must be made to the seals and valves associated with liquid propellants. These propellants are further subdivided into monopropellants (the oxidizer and fuel are in the same container) and bipropellants. Each requires a pumping method to combine them, which is achieved using one of a few typical ways.[1]

Figure 1. HELLFIRE missile. MQ-9 Reaper firing HELLFIRE missile filled with minimum-smoke cross linked double base (XLDB) solid propellant

The last and most recently developed propellant are those used in hybrid systems involving a liquid and a solid phase. In these systems, the oxidizer is in one phase, and the fuel in kept in another phase and then they are combined. This rocket system can outperform both solid and liquid designs, and the high temperature combustion occurs in a small area. They are also cheaper than other types. However, they are the more complicated of propellant systems and not extensively used for this reason.[1] Regardless of the propellant in the rocket system, propellant performance is measured the same way.

1.1.2 Solid Propellant Chemical Energy

When measuring the energy characteristic of a propellant, two important properties are evaluated: heat of combustion (ΔH_c) and specific thrust or specific impulse (I_{sp}). The amount of ΔH_c is the potential chemical energy released from the propellant mixture at 25°C. Since propellants typically burn far above that temperature, the full chemical potential is not achieved. The second unit of measure, I_{sp}, measures both the energy source but also the efficiency of the working substance. Since calorimetry is temperature and pressure dependent, I_{sp}, per unit mass, is most commonly used when comparing propellants.[2]

To determine the I_{sp} of a propellant, first the exit velocity of the propellant combustion must be determined. The ideal exhaust velocity equation is used to calculate the V_e (Equation 1 below):

$$V_e = \sqrt{\left(\frac{2k}{k-1}\right)\left(\frac{R^* T_c}{M}\right)\left(1 - \left(\frac{P_e}{P_c}\right)^{(k-1)/k}\right)} \qquad \text{(Equation 1)}$$

In the above equation, k is the specific heat ratio, R^* is the ideal gas constant (8,314.4621 J/kmol)-K, T_c is the combustion temperature, M is the average molecular weight of the exhaust gases, P_c is the combustion chamber pressure, and P_e is the pressure at the nozzle exit. Once determined, the I_{sp} can be calculated by the V_e divided by gravitational attraction of the earth (g_e) found in Equation 2 below.[2]

$$I_{sp} = V_e/g_e \qquad \text{(Equation 2)}$$

However, specific impulses can only be compared when the expansion ratio of the produced gases are the same. Using the ideal gas law, as the number of moles increases, so does the pressure or volume of the gas produced, so complexes that combust and produce light weight gas products have typically been desirable when developing propellants.

Lastly, the amount of oxidant in a propellant is commonly measured to ensure as complete combustion as possible is achieved without requiring excess external oxidation (usually done by oxygen). Ideally, propellants have a stoichiometric value of 1, with enough oxidant to completely convert all the reactants.

Of interest to this research manuscript is also the measurement of the combustion rate of a propellant. The combustion rate is the rate at which exhaust gases are produced, and this in turn decides the flow rate through the nozzle and is typically measured in mm/second or inches/second. Burn rates within a rocket motor are typically temperature and pressure sensitive. However, one particular burn rate phenomenon sometimes called the "super-rate", "plateau", or "mesa effect", alter combustion chamber pressure as it relates to burn rate. This phenomenon, discussed later in the chapter, can have profound effects on double-base propellant.

1.1.3 Double-Base Propellants

Solid propellants for rockets and missiles are either double-base (DB), modified double-base (MDB) or composite modified double-base (CMDB).

All DB propellants possess a sufficient oxygen balance within their structure to transform into gaseous products without the need for external oxygen. DB propellants are prepared one of three ways and end in a homogenous solid plastic.

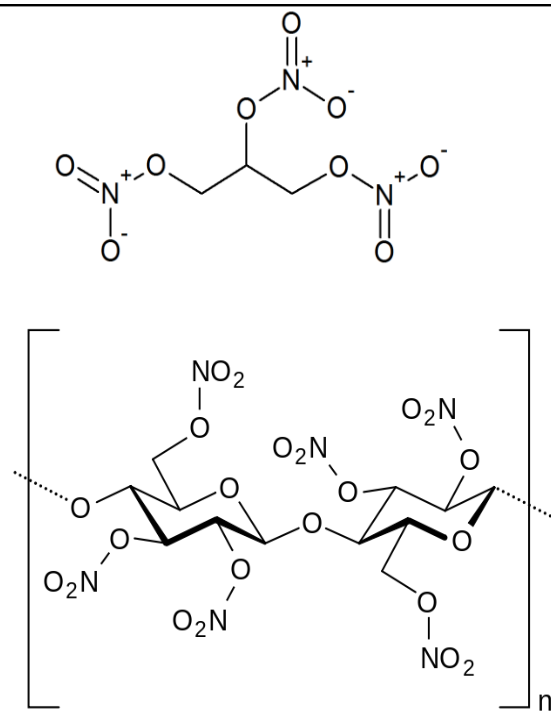

Figure 2. Structures of NG and NC. Structures of nitroglycerine (top) and nitrocellulose (bottom)

Modern double base propellants consist of: 50% nitrocellulose (NC) (12.6% nitrogen), 34.9% nitroglycerine (NG), 10.5% diethyl phthalate, 2% 2-nitrodiphenylamide, 1.2% Lead Salicylate, 1.2% lead 2- ethyl hexoate, .2% candelilla wax (Figure 2).[3] Modified double-base propellants exhibit better performance and are typically double-base propellants with the addition of HMX, triactin, ammonium perchlorate or aluminum metal. Composite propellants are a composite polymer with ammonium perchlorate as an oxidizer. All three are in frequent use. A specific type of composite modified double-base propellant commonly used in modern military missiles are called cross-linked (XLDB), which is when the nitrocellulose is linked to a polymer chain to a binder greatly increasing the tensile strength and structural integrity of the propellant.[4]

Double-base was coined as a term to use for propellants that use primarily 50% NC and 50% NG, but it also implies "smoke-less propellant". Early propellants were simply gun powder formulations and created a large amount of black smoke when burned, and users did not have accurate control of the combustion reaction. The grain size of the powder effects burn rates, so careful grain size control and building specific grain shapes allowed for better control over reaction speed and evenness. Traditional double-base propellants without energetic additives produce much less noticeable gas products then modified or composite, making them useful for military applications when obscuring the source and path of the missile is required.

Exploring the specific composition of double base propellants provides an understanding the role of each chemical in the compound. However, different types of double-base propellants are all a blend of fuel, oxidizer, binders, plasticizers and ballistic modifiers, usually produced in a single batch. Additionally, many chemical compounds play more than one role within the propellant. However, general categorization can be made of the six or so core components in a typical double-base military propellant:[5]

(1) The nitroglycerine provides the fuel and oxidizer for the propellant. It is relatively stable, has high potential chemical energy and is relatively easily mass produced (affordable).

(2) The nitrocellulose is primarily used as an energetic binder to hold the propellant together.

(3) The diethyl phthalate is an auxiliary plasticizer.

(4) The 2-nitrodiphenylamide (NDPA) is a stabilizer. The nitro groups in the propellant reduce the autocatalytic decomposition of nitrocellulose within the propellant. With the addition of NDPA, the shelf life of the DB propellant is significantly increased.[6]

(5/6) The Lead Salicylate and lead 2- ethyl hexoate are added as a ballistic modifier and pivotal to the burn rate phenomena observed that are discussed at length in this thesis and critical to the research hypothesis presented later.

(7) The candelilla wax is used as a lubricant and help with molding.

There has been considerable research in improving each of these components in a variety of ways. For example, fuels have been mixed with oxidizers to improve performance (such as ammonium perchlorate). Different stabilizers have been researched to lengthen storage times and reduce toxicity.[7 However], arguably the largest amount of research resources have been dedicated to the improvement of the ballistic burn rate modifiers and catalysts.

1.1.4 Burn Rate Catalysts and Burn Rate Modifiers

Burn rate catalysts (BRCs) or burn rate modifiers, are essential ingredients to many solid DB propellants. They enhance the burning character of the propellant and are responsible for eliminating much of the smoke produced. Copper organic chelates or lead-iron double metal chelates make good BRCs and greatly enhance burn rates. Ferrocene derivatives containing alkyl, acyl, and ester functional groups demonstrate additional increased performance of butyl hydroxide propellants containing ammonium perchlorate (AP), aluminum powder, and RDX.[8,9] Unfortunately, ferrocene BRCs migrate ferrocene-based BRCs migrate within the propellant, which reduces shelf life and alters designed burning parameters. Recent research has been conducted to find ferrocene based BRCs with little movement within the propellant under storage conditions.[9]

To tailor the propellant grain and thrust requirements, substances such as lithium fluoride are occasionally added to slow the burn rate of a propellant. Furthermore, leaded compounds are also added as a ballistic modifier to propellants but for an entirely different reason.

Lead was discovered in WWII to produce very desirable ballistic effects on burn rate and pressure, when added to double-base propellants. It was observed that small quantities of lead, when added during the propellant excursion process, increased burn rates at low pressures. This “super-rate” phenomena were observed in conjunction with “plateau burning” or “platonizing” (burn rate independent of pressure) and “mesa burning” (burn rate decreases as pressure increases).

1.2 Burn Rate Phenomena

1.2.1 ‘Super-Rate’, ‘Plateau’, and ‘Mesa’ Phenomena

Burn rate is profoundly affected by chamber pressure. The usual representation of the pressure dependence on burn rate can be demonstrated in Saint-Robert's Law;

$$r = ap^n \quad \text{(Equation 3)}$$

where r is the burn rate, a is the burn rate coefficient, n is the pressure exponent, and p is the combustion chamber pressure. The values of a and n are determined experimentally for a propellant formulation and cannot be theoretically predicted. It is important to realize that a single set of a and n values are typically valid over a distinct pressure range.[11]

Typical burn rates increase linearly with an increase in pressure (Figure 3).[10] However, under plateau conditions a burn rate phenomena occurs, and the burn rate does not increase with pressure. The pressure exponent (n), is approximately zero for plateau

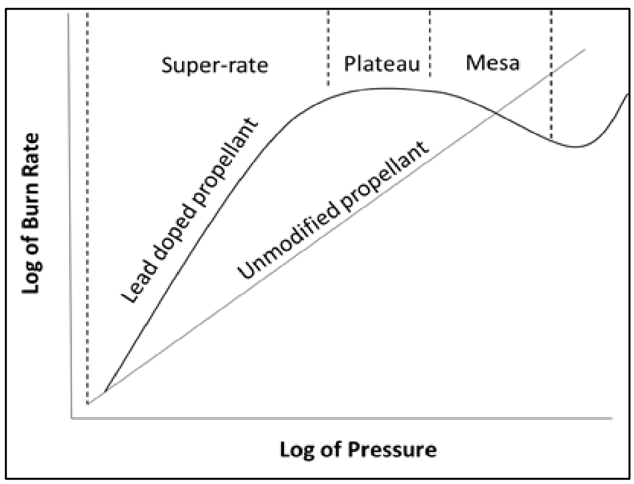

Figure 3. Sketch of 'n'. Log burn rate versus log of pressure

burning and is negative for mesa burning, as shown below in Figure 6. The physical and chemical properties of the lead and amount used greatly effect pressure exponent of super-rate, plateau, and mesa burning. Furthermore, as the density of the NC-NG compound is varied, or heat of explosion is altered, the pressure exponent of the burn rate (n) remains unchanged (~0.64).[11]

With lead-catalyzed propellant, super rate burning occurs when n is greater than 0.8 at low pressures so motor performance is improved immediately after ignition when burn rate is higher at low pressure than unleaded propellant. However, when 'n' is greater than 1, burning can become erratic so the value n needs to be arrested, and fortunately a plateau zone is observed where the burn rate is independent of the pressure in the combustion chamber. Then, burn rate becomes negative at higher temperatures, helping significantly reduce stress on the rocket motor.

But not all Pb compounds produce these burn rate changes. For example, several lead compounds, such as $PbBr_2$, PbI_2, and $PbCl_2$, do not. But Lead 2-ethylhexoate and lead salicylic acid do.[11] The exact reason for this phenomenon is yet to be conclusively determined.[12]

1.2.2 Double-Base Combustion Reactions

Double-base propellant combustion is achieved over several sequential chemical reactions that take place within different burn "zones" (Figure 4).

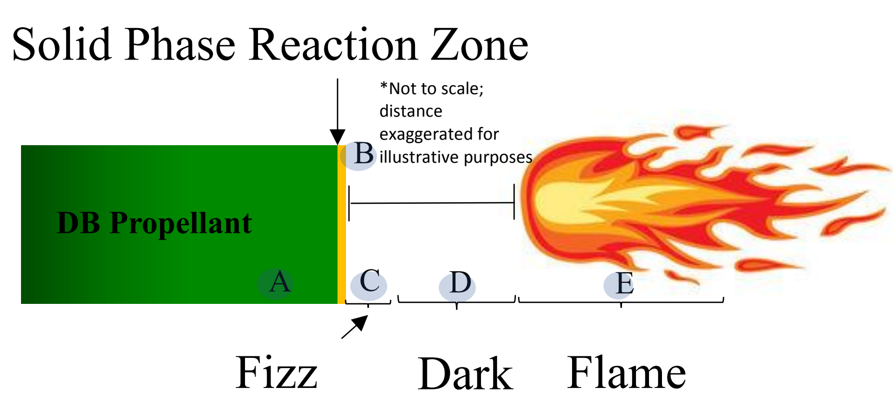

Figure 4. Wave zones. Double-base propellant combustion wave

In zone A, the propellant increases in temperature but does not start to degrade until the solid phase reaction zone, (B) when enough energy is applied to break chemical bonds within the fuel. The atoms recombine to form NO_2, aldehydes, and NO, making the reaction exothermic. In the fizz zone (C) nitrogen dioxide, aldehydes and other C, H, O species react to produce nitric oxide, carbon monoxide, water, hydrogen, and carbonaceous materials. This reaction process occurs very rapidly just above the burning surface. In the dark zone the same reactions as (D) take place but much slower. Finally, in the flame zone (E), N_2, CO, CO_2, H_2O and H_2 are formed, with the formation of N_2 releasing much of the energy in the form of heat and completing the reaction.[11]

However, lead doped propellants create lead oxides at the solid phase reaction zone, creating conditions for super-rate burning. Sharma et al., proposed that metallic lead reacts with NO_2 to form lead oxide (Sharma observed this molecule in XPS studies). Sharma concludes that the lead oxides greatly increase the oxidation rate of carbon by five orders of magnitude producing more CO_2 and thus "super-rate" burning.[13]

Similarly, Sharma supports conclusions from Otto et al., that Pb(s) eventually saturates the burning surface, plugging gaps within the carbon structure on the surface and slowing the burn rate regardless of pressure, creating the "plateau" and "mesa" regions.[14]

This is a simplified version of one hypotheses of how lead effects DB combustion. The chemistry is not fully understood and still debated, with numerous hypotheses attempting to answer this question.

1.3. Research Question

In any solid rocket motor design, the type of solid propellant is the largest performance factor. Solid propellants should exhibit a high I_{sp}, be a dense matter, have predictable burning characteristics, be affordable, have a low burning profile, possess a long shelf life and importantly, produce desirable thermal effects. However, toxicity has become a concern as well.

Since the 1990s the Department of Defense has attempted to replace the lead used in ballistic modifiers and replace it with a less toxic element to decrease handling precautions, ease recycling of propellants and reduce personnel exposure. Several other chemical elements have been pursued, including tin, bismuth, and copper in achieving the same effects as lead, but with limited success.[15] Most uses for DB propellants are for military application and have specific ballistic requirements that have yet to be successfully duplicated by a complete substitution of lead. A useful substitute to create the same ballistic effects appears to be a mix of both copper and bismuth.[15] This is an obvious area of research need, and resources are available. However, the chemistry is poorly understood and already routinely studied by numerous groups.

BRCs are investigated and new ballistic modifiers and stabilizers have been developed. The need for better platonizing agents always exists, as does the need to increase propellant performance. One such way previously identified, was by using the same chemical compound to fill multiple roles, reducing weight and increasing performance (as in the case of energetic binders).

After close examination of these recent efforts, a research gap was identified. A literature review didn't reveal any efforts to react various metals with industry used propellant stabilizers. Although together they make up only a small fraction of total DB propellant weight (< 4%), perhaps a combination of both could possibly yield results that produce a long list of desirable qualities. Successful synthesis of unleaded complexes could create a pathway to make less toxic additives that the DoD has been trying to achieve for almost 30 years. A thesis question was formed and research focus developed: *could propellant stabilizer and a metal as ballistic modifier be combined to create a superior double-base propellant additive?*

1.4 References

1. Ramnarace, J. *Rocket Propellant Technology*, Page publishing: New York, NY, 2015.

2. Braeunig, R. A., Rocket and Space technology, http://www.braeunig.us/space/propuls.htm (accessed 5 January 2017).

3. Composition of Type N5 Nitrocellulose-based Double Base Propellant, courtesy of Island Pyrochemical Industries, http://www.islandpyrochemical.com/military/rocket_propellants.php (accessed 10 December 2016).

4. Bhat, V.K.; Singh, H. Cross-Linked Slurry Cast Composite Modified Double Base Propellants: Mechanical Properties. *Def Sci J.*, **1987**, 37,1, 39-44.

5. Yang, V. Thakre, P. Encyclopedia of Aerospace Engineering, Blockley, R. and Shyy, W., Ed; John Wiley and Sons, Ltd: **2010**.

6. Apatoff, J. B.; Norwitz, G. *Role of Diphenylamine as a stabilizer in propellants; analytical chemistry of diphenylamine in propellants*; US Army Armament Command, Test Report T73-12-1, 1973.

7. Tunestål, E.; Hafstrand, A.; Lindborg, A.; Krumlinde, P.; Ek, S.; Goede, P.; Schragen, C. New stabilizers for NC-propellants Evaluated in Rocket Propellants. FOI, Swedish Defense Research Agency, Department of Energetic Materials and Modelling, SE-147 25 Tumba, Sweden.

8. Zain-ul-Abdin, L.W.; Yu, H.; Saleem, M.; Abbasi, N.; Ullah Khan, R.; Ullah, R. S.; Haroon, Mu. Synthesis of ferrocene-based saccharides and their anti-migration and burning rate catalytic properties. *RSC Adv.*, **2016**, 6, 97469–97481.
9. Gao, J.; Wang, L.; Yu, H.; Xiao, A.; Ding, W. Recent Research Progress in Burning Rate Catalysts. *Propellants, Explos. Pyrotech*. **2011**, 36, 404 – 409.

10. Sketch redrawn from Kubota, N. *Propellants and Explosives*, WILEY-VCH Verlag GmbH & Co. KGaA, Weinheim, 2007.

11. Kubota, N. *Propellants and Explosives*, WILEY-VCH Verlag GmbH & Co. KGaA, Weinheim, 2007.

12. Fifer, R.A. *Workshop Report: Fundamental Reactions in Solid Propellant Combustion;* ARBRL-TR-02166; 1979.

13. Sharma, J.;Wilmot, G.B.; Campolaattro, A. A.; Santiago, F. *Combustion and Flame*, **1991**, 85, 416-426.

14. Otto, K.;Lehman, C.;Bartosiewicz, L.;Shelef, M. *Carbon*. **1982**, 20, 243-251.

15. Magill, B. T.; Nauflett, G. W.; Furrow, K. W. *Lead-Free Double-Base Propellant for the 2.75 Inch Rocket Motor;* 20000116525; Cocoa Beach, FL, 2000.

CHAPTER 2

LITERATURE REVIEW OF BALLSITIC MODIFIER AND STABILIZER

2.1. Ballistic Modifiers

There have been decades of research into developing better lead containing compounds for plateau/mesa burn rate effects and in burn rate catalysts. Furthermore, aggressive research efforts have been underway since the 1990s to find alternatives to lead – with some success. It would be impossible to summarize them all here in a literature review, but an assortment of research efforts is summarized that were both noteworthy and significant to the research undertaken to answer the thesis question.

2.1.1 Leaded Ballistic Modifiers

Extensive research into using lead complexes for burn rate modifiers began in the 1950s and carries through today.[1] Over time, and likely due to financial factors as much as performance, several different lead ballistic modifiers are used today. More conventional and older compounds being: lead salicylate, lead 2-ethyl heoxate and lead beta resorcylate. However, several lead-copper compounds are in use for many military applications: LC-12-0, LC-12-5, LC-12-6, LC-12-7, LC-12-10, LC-12-15 and LC-12-20.[2] A quick investigation of LC-12-15 for example, reveals a copper content between 10-13%, and lead of 35.8%-39.4% with salicylic acid and resorcyclic acid making up all but 4% of the rest.[3]

A recently created lead crystal $[Pb_2(phen)_4(CO_3)][FcTz)_2 \cdot phen \cdot 9H_2O$ was synthesized in 2015 as a potential burn rate catalyst due to the various drawbacks exhibited by commercially available ballistic modifiers *n*-butytlferrocene, *tert*-butytlferrocene and 2,2-bis(ethylferrocenyl)propane.[4] The $[Pb_2(phen)_2(H_2O)_3](FcTz)_2{\cdot}H_2O$ (Figure 5), crystallizes in the triclininc *P*-1 spacegroup. It contains two Pb (II) cations, four phenol ligands, one carbonato ligand, two FcTz anions, one phenol molecule and nine lattice water molecules.

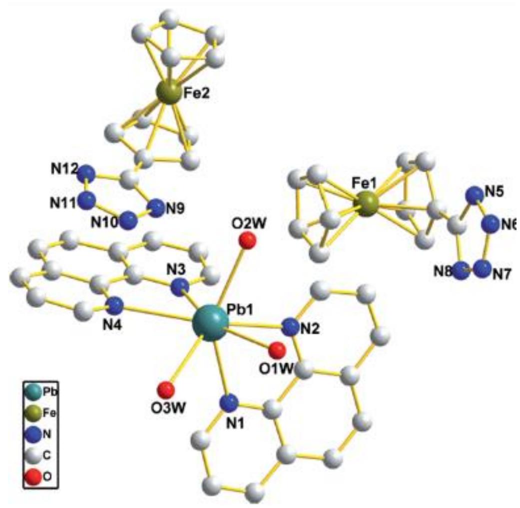

Figure 5. Wang crystal. Crystal structure of $[Pb2(phen)_2(H2O)_3](FcTz)_2{\cdot}H_2O$ (from Wang, et al.)

The authors propose that arrangement of atoms around the Pb center suggest that a hole exists around the metal ion that is occupied by a stereo active lone pair of electrons on the Pb(II) ion. This group also successfully synthesized other transition metal complexes, $[Cu_2(bpy)_2(FcTz)_4]{\cdot}2C_2H_5OH$, $[Cu(phen)_3](FcTz)_2{\cdot}8H_2O$, $[Ni(phen)_3](FcTz)_2{\cdot}9H_2O$ and $[Co(phen)_3]FcTz){\cdot}9H_2O$. Each complex comprised several water molecules in the lattice, leading the authors to believe that packing of each crystal was influenced by strong intra- and intermolecular hydrogen bonds. Furthermore, each complex stability is increased by the π-π interaction between phenol and Cp molecules.[4]

Similar stabilization effects were observed in the manganese-containing crystals the Wang group produced $[Mn(phen)_2(H_2O)_2](FcTz)_2$ and $[Mn(bpy)(H_2O)_4](FcTz)_2$ for burn rate modification.[4] However, in the case for each of these crystals, although structurally relevant to the chemistry in this manuscript, they were specifically designed for use as catalysts for AP and RDX augmented solid propellants. It was not mentioned if plateau/mesa effects were observed with these structures since this was not the focus of the research.

In 1988 the burn rates of lead and copper salts were studied in RDX doped composite modified double-base propellant (CMDB) by Raman and Singh.[5] It was reported that lead methylene disalicylate (LMDS), basic copper salicylate (BCS), cobaltic oxide and lead stannate produced higher burning rates over non-doped CMDB by 10%–16% and burn rates were raised even higher when the CMDB was primarily nitramines and not AP. Fluorides of chromium, iron and lead did not increase the burn rates and inclusion of lead salts and carbon black or transition metal oxides only produced a small burn rate increase. Importantly, none of the complexes studied exhibited a plateau or mesa effect.[5]

2.1.2 Unleaded Alternatives

As previously mentioned, the Department of Defense has attempted to remove lead from ballistic propellants since the 1990s. Several research efforts have been made with that goal in mind.

Since their discovery in the 1950's, ferrocene derivatives have been used as solid propellant as burn rate catalysts.[6] These iron complexes produced superior burn rates and could be used in larger quantities over previous compounds, such as iron oxide. However, a disadvantage of ferrocene burn rate additives is their tendency to migrate within the propellant affecting, mechanical and chemical properties during storage.[6] Several ferrocene compounds were developed over the past 60 years. *tert*-Butyl ferrocene (TBF), catocene, 2,2-bis(butylferrocenyl) propane (BBFPr) and 2,2-bis(butylferrocenyl) pentane (BBFPe) are but a few examples, all developed with high burn rate properties.[6] These compounds, however, were not evaluated for, nor expected to demonstrate plateau/mesa effects due to the inability of iron metal complexes to exhibit that burn rate phenomena.

Research by Deisyuk and Demidova found lead, tin, titanium oxides and bismuth also to increase burn rates of DB propellants, providing optimism that these elements could also be used to replace lead.[7] Unfortunately in their research, plateau/mesa effects were not investigated using these metals.

One successful unleaded compound was made for 2.75-inch rockets. The Navy Surface Warfare Center (NSWC), Radford Army Ammunition Plant, and Alliant Tech systems created a lead-free double-base ballistic modifier with plateau and mesa burn rate characteristics. The double-base additive developed consists of four components: 1.5% bismuth subsalicylate, 1.0% copper salicylate, 0.77% copper stannate, and 0.1% carbon black. This compound's specific impulse output was not an exact match for existing propellant within the 2.75-inch Rocket Motor (NOSIH-AA-2), but inventors believed a close enough match to be an acceptable replacement. However, this lead-free compound exhibits a significant drawback from current propellant: The stabilizer within the lead-free compound exhibited a much higher rate of depletion than current NOSIH-AA-2. Although the analysis from the group demonstrated that a mixture of bismuth subsalicylate and copper salicylate reduced the depletion rate of the stabilizer by half, the presence of the copper salicylate catalysed the decomposition of the nitrocellulose. Although patented, efforts were underway to protect the ballistic modifier from the nitrocellulose with a coating to make it a truly viable alternative to NOSIH-AA-2.[2]

The ability to eliminate lead entirely from ballistic modifiers may not be possible. A research group at the Naval Surface Warfare Center conducted XPS studies between leaded and unleaded DB propellant. What was observed corroborated earlier research: that lead plays two pivotal roles in producing plateau/mesa effects:[8] First, it creates soot on the burning surface of the propellant – a requirement for pressure and burn rate effects. Secondly, the lead increases the oxidation rate of the of carbon by five orders of magnitude for super-rate burning.[8] It was suggested by Otto et al. that lead eventually becomes saturated at the burning surface thereby plugging holes within the soot carbon structure and arresting the super-rate burning.[9] The Navy group later observed that during the onset of plateau/mesa burning, there was a sudden decrease in lead to carbon ratio suggesting that the amount of lead on the burning surface is a key driver of plateau/mesa burn charateristics.[8]

Given this lack of clarity over the combustion chemistry, and inability to find a suitable unleaded alternative – lead or lead containing reactants generally continue to be a requirement for ballistic modification when super-rate and similar burn rate effects are desired.

2.2 Double-base Propellant Stabilizers

The nitrocellulose component of double-base propellants undergoes an autocatalytic decomposition process whereby it decomposes to form NO and then evolves NO_2 with contact to air. This process creates heat and promotes the degradation of the propellant. The propellant grains show a discolored roughened surface at the ends and edges of the grains.[10] To prevent that process and to increase shelf-life and maintain chemical integrity of the propellant, a few stabilizers are commonly used: Diphenlamine (DPA), 2-nitrodiphenyl amine (NDPA), Centralite I&II and Akardite I&II.[11] However, these stabilizers form N-nitrosoamines within the propellant, which are toxic. Some research has been conducted to find nitrogen free, aromatic free stabilizers.

Researchers at the Swedish Defence Research Agency successfully synthesized a few unique stabilizers in 2015 that appear as good replacements.[11] Stab-5 (bis-(2,6-dimethoxyphenol)) (Figure 6) and retinyl acteate (Figure 7), were two produced that had similar burn characteristics, and exhibited the stabilizing properties as conventional stabilizers without toxic by-product.[11]

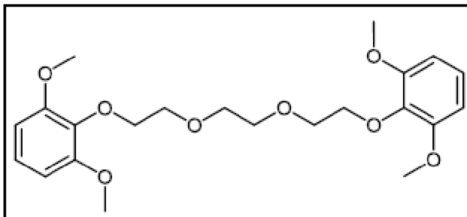

Figure 6. Stab-5

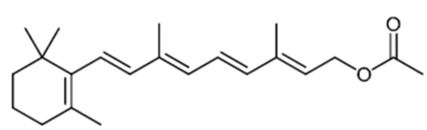

Figure 7. Retinyl acteate

Nevertheless, although promising, non-conventional DB propellant stabilizers do not appear to be currently used often, if at all.

2.3 Methodology

Conclusions were drawn from previous efforts and influenced the research methodology. First, although a demand exists, the ability to replace lead with other elements appears an extraordinary task, if even possible. Therefore, lead would be included in synthesis of a new organometallic complex. Secondly, given the novelty in recent stabilizers, the research would include common DB propellant stabilizers to provide practicality if successful.

The Zdilla research lab was very familiar with Mn clusters and their synthesis using $M(N(SiMe_3)_2)$ (where M=metal) (Figure 8).[12]

The metal cation is fungible, with dozens of metals having been reported to be coordinated to bis(trimethylsilyl)amide.[12] Metal bis(trimethylsilyl)amide complexes are nonpolar and have low lattice energies. They are soluble in a range of nonpolar organic

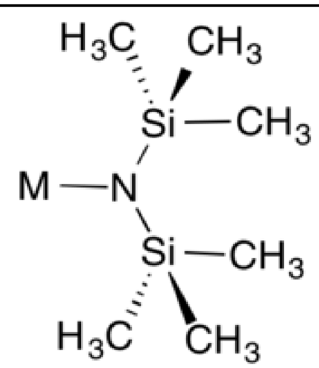

Figure 8. Metal reactant. Metal with attached bis(trimethylsilyl) ligand

solvents, simplifying synthesis. Furthermore, these complexes are strong bases and react with weak protic agents, presenting easy chemistry targets for reactions, and facilitating protolytic ligand replacement reactions. Unfortunately, they are also air-sensitive, and react with water so need to be used in anhydrous environments. Using previous literature for burn rate modifiers mentioned above, and chemical similarity to lead, four metal bis(trimethylsilyl)amides were planned as reactants: lead, zinc, tin, and bismuth.

The choice for a ligand was to use a commonly used double-base stabilizer. N-Methyl-4-nitroaniline is an antiquated yet previously used common stabilizer in older propellants, but to maintain the methyl and nitro groups when reacting with the metal bis(trimethylsilyl)amide, a variant, 4-methyl-3-nitroaniline was purchased and used.

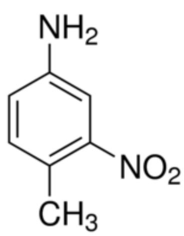

Figure 9. 4-methyl-3-nitroaniline

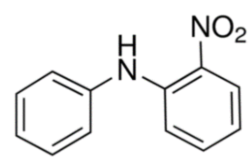

Figure 10. 2-Nitrodiphenylamine

A common and more modern stabilizer was chosen as a second stabilizer reactant, 2-Nitrodiphenylamine (NDPA) (Figure 10). As with N-Methyl-4-nitroaniline, this stabilizer offers an easy target in the deprotonation of the amide.

In summary, an effort was made to react four metal bis(trimethyl)amides with two stabilizer ligands in hopes of achieving a new complex that: (1) serves as both burn rate modifier with super-rate, mesa and plateau rate burn characteristics within useful pressure ranges, (2) stabilizes the DB propellant as well or better than existing compounds such as NDPA, (3) possibly achieve goals one and two using an unleaded complex.

2.4 References

1. A. T. Camp, Patent US 3,088,858, 1963.

2. Magill, B. T.; Nauflett, G. W.; Furrow, K. W. *Lead-Free Double-Base Propellant for the 2.75 Inch Rocket Motor;* 20000116525; Cocoa Beach, FL, 2000.

3. Ballistic Modifier LC-12-15 Mil Spec, courtesy of parchem, www.parchem.com/Ballistic-Modifier-LC-12-15-Mil-Spec-getpdf-013001.aspx (accessed 15 March 2017).

4. Wang, C.; Li, J.; Fan, X.; Zhao, F.; Zhang, W.; Zhang, G.; Gao, Z.; 5-Ferrocenyl-1H-tetrazole-Derived Transition-Metal Complexes; Synthesis, Crystal Structures and Catalytic Effects on the Thermal Decomposition of the Main Components of Solid Propellants, *Eur. J. Inorg. Chem.*, **2015**, 1012-1021.

5. Raman, K.V., Singh, H., Ballistic Modification of RDX-Based CMDB Propellants, *Propellants Explos. Pyrotech.,* **1988**, 13*, 5*, 149-151.

6. Zain-ul-Abdin, L. W.; Haojie Y.; Muhammad S.; Nasir A.; Rizwan, U.K.; Raja S.; Haroon, M. and U.; Synthesis of ferrocene-based saccharides and their anti-migration and burning rate catalytic properties. *RSC Adv.*, **2016**, 6, 97469–97481.

7. Denisyuk, A.P., Demidova, L.A., Effect of Some Catalysts on Combustion of Double-Base Propellants, *Combustion, Explosion, and Shock Waves,* **2004**, 40, 3 311-318.

8. Sharma, J., Wilmot, G.B., Campolattaro, A.A., Santiago, F., XPS Study of Condensed Phase Combustion in Double-Base Rocker Propellant with and without Lead Salt-Burning Rate Modifier, *Combustion and Flame*, **1991**, 85, 416-426.

9. Otto, K., Lehman, C., Bartosiewicz, L., Shelef, M., *Carbon*, **1982**, 20, 243-251.

10. Apatoff, J. B.; Norwitz, G. *Role of Diphenylamine as a stabilizer in propellants; analytical chemistry of diphenylamine in propellants*; US Army Armament Command, Test Report T73-12-1, 1973.

11. Tunestål, E.; Hafstrand, A.; Lindborg, A.; Krumlinde, P.; Ek, S.; Goede, P.; Schragen, C. New stabilizers for NC-propellants Evaluated in Rocket Propellants. FOI, Swedish Defense Research Agency, Department of Energetic Materials and Modelling, SE-147 25 Tumba, Sweden.

12. Hamilton, C.R.; Gau, M. R.; Baglia, R. A.; Mc Williams, S. F.; Zdilla, M. J.; Mechanistic Elucidation of the Stepwise Formation of a Tetranuclear Manganese Pinned Butterfly Cluster via N-N Bond Cleavage, Hydrogen Atom Transfer, and Cluster Rearrangement, *Journal of the American Chemical Society*, **2014**, 136, 17974-17986.

CHAPTER 3
RESULTS/DISCUSSION

*Note: all experimental details can be found in the final chapter, chapter 5 of this manuscript.

3.1. Reagents

Formation of metal bis(trimethylsilyl)amides, or $M(N(SiMe_3)_2)$, reactants were generally successful using the commonly-used salt-metathesis reaction of:

$$K(N(SiMe_3)_2) + MR \longrightarrow M(SiMe_3)_2 + KR \text{ (where M=metal, R=halogen)} \quad \text{(Equation 4)}$$

$Pb(N(SiMe_3)_2)$ was not available commercially so synthesis from $Na(N(SiMe_3)_2)$ and PbI_2 was required. Approximately 12g (47% yield) was successfully obtained and characterized from indexing the yellow crystals using XRD.[1] It was stored in -30°C in an oxygen and moisture free environment and used in many future reactions.

$Sn(N(SiMe_3)_2)$ was available commercially but was backordered and had a long delivery delay. Therefore, it was ordered but was also synthesized in the lab for expediency. 3.34g (31% yield), of $Sn(N(SiMe_3)_2)$ was successfully synthesized and rudimentarily characterized by comparing FTIR spectra of the synthesized and delivered commercial reagent. Further and more conclusive characterization was not performed because: (1) $Sn(N(SiMe_3)_2)$ commercial product was made available and (2) subsequent reactions were not successful making further analysis, time prohibitive. At room temperature, it is an orange red liquid.

$Zn(N(SiMe_3)_2)$ was not commercially available. As a cloudy white solid, $Zn(N(SiMe_3)_2)$ melts are room temperature, but product appearance and melting point matched previously reported chemical properties.[2] 5.496g (49% yield) was produced.

Another $M(N(SiMe_3)_2)$ previously discussed as a reactant was $Bi(N(SiMe_3)_2)$. 1.51g was produced (41% yield). It dried to a primarily yellow powder indicative of the substance. It was characterized by matching melting point range to literature.[3]

3.2 Products

A total of 36 reactions were attempted by combining various metal reagents and the two previously mentioned propellant stabilizers. The end state of each reaction was to produce stable crystals of metal/stabilizer complexes that could be characterized by a minimum of three experimental techniques and suitable for testing at a collaborating lab for burn rate and pressure effects.

The crystals were grown by a vapor diffusion technique in a double vial apparatus. This method was by far the most effective crystal growing method during this research, and used a two-solvent system. The choice in solvents is to ensure that they are miscible and a significant difference in polarity is preferable. In most reactions, the products were dissolved in THF and aliquoted into an inner sample vial and pentane placed in the outer scintillation vial and sealed. Varying the temperature during concurrent attempts ensured that the crystallization proceeded at different speeds. However, when reactions created a color change, and formed product without a crystal, additional crystallization techniques were employed: slow cooling, and convection (by heating the bottom of the solution in an NMR tube). Unfortunately, these attempts never succeeded where vapor-diffusion had failed.

Numerous attempts with various metals and crystallization techniques (usually conducted both at room temperature and at -30˚ C), yielded two useful crystal structures. Two novel complexes were synthesized, while pursuing precursors for developing a new family of dual stabilizer/ballistic modifiers, and in the process discovered an extremely high-energy-density lead-based heterocubane compound.

3.2.1 Tetrakis(μ3-(4-methyl-3-nitrophenyl imido lead (II)))

A 1:1 stoichiometric reaction of lead bis(trimethylsilyl)amide with 4-methyl-3-nitroaniline produced tetrakis(μ3-(4-methyl-3-nitrophenyl imido lead (II))) (**1**). The reaction is illustrated in Equation 5.

$$4\ Pb[(N(Si(CH_3)_3)_2)] + 4[C_6H_5(CH_3)(NH_2)(NO_2)] \xrightarrow[23^{\circ}C,\ 24\ hrs]{THF}$$

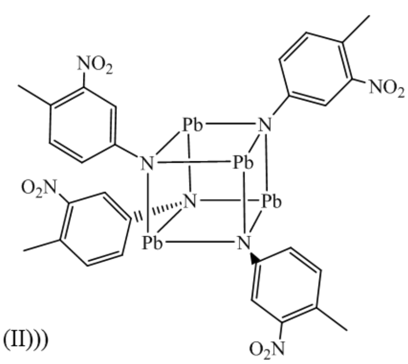

Tetrakis(μ3-(4-methyl-3-nitrophenyl lead (II)))

(Equation 5)

Single-crystal X-ray diffraction analysis was performed on the dark red or rust colored crystals, and **1** is a triclinic system with the space group of *P*-1. It has four Pb^{+2} ions, surrounded by four 2-nitromethyl aniline ligands. A thermal ellipsoid plot is shown below (Figure 11).

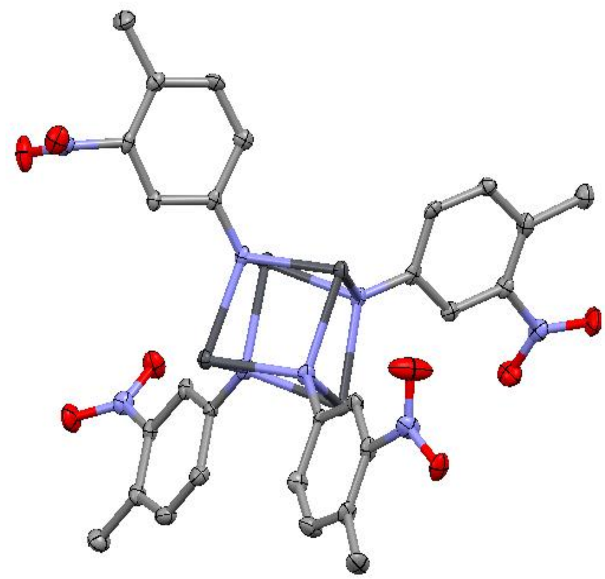

Figure 11. Thermal ellipsoid plots of **1**. Ellipsoids set at 50% probability level, hydrogens and THF solvate omitted for clarity.

The cubane structure of the Pb and N atoms was not found readily in literature and appear unique. The tetrakis structure is distorted, with bond angles varying between atoms within the cube from 78.6° to 100.0°. This distortion is likely from NO_2 groups weakly coordinating to the Pb of adjacent clusters. However, no π-π stacking is present in the crystal. The N-C bond distances are ~ 1.4 Å, slightly shorter but close to expected bond distances, and all C-C bonds are of typical length. Two ligand aromatic rings are perpendicular to the other two, about equidistant apart ~4.8 Å, and are not so large as to sterically hinder the Pb cation.

Different solvents were attempted to dissolve **1,** with only pyridine being capable. **1** was not soluble in THF, ACN, HMDS, benzene, toluene, pentane or ethanol. However, using deuterated pyridine produced ^{1}H NMR spectra that supports the proposed structure and is found below in Figure 12.

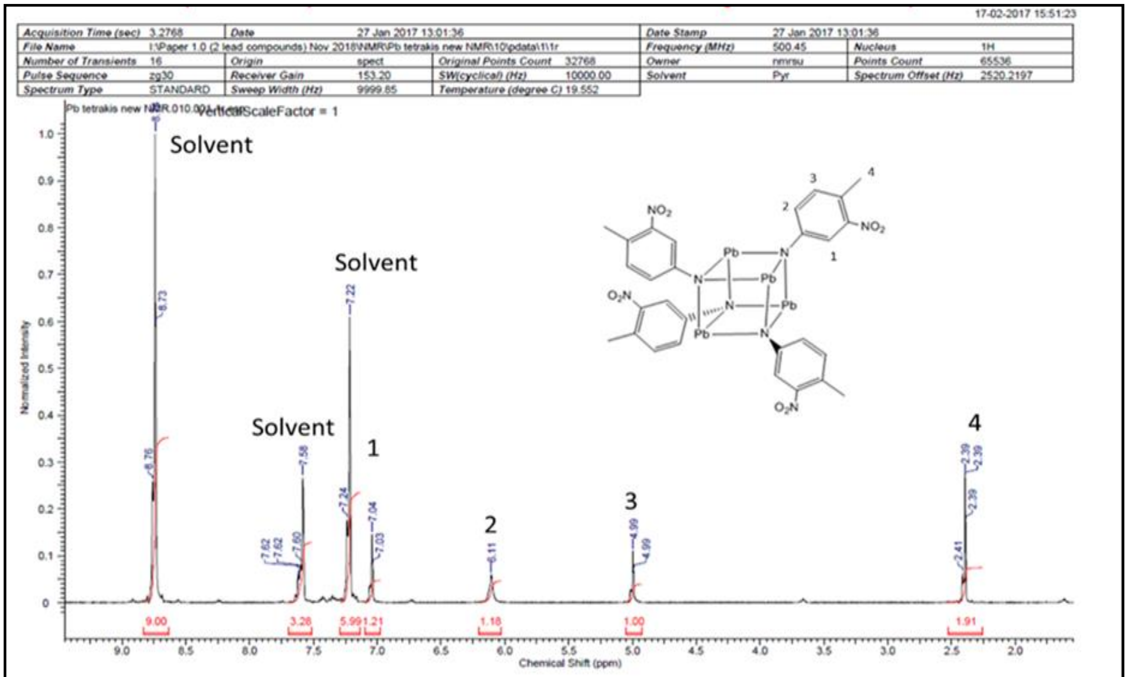

Figure 12. ^{1}H NMR spectra of **1**

CHN analysis supported the structure with one co-crystalized THF molecule within the lattice (not uncommon). Theoretical for $C_{28}H_{24}N_8O_8\,Pb_4\cdot 1\,(CH_2)_4O$: C, 25.60%; H, 2.15%; N, 7.46%, and experimentally found: C, 25.44%; H, 1.99%; N, 7.41%.

The IR spectrum provides limited supporting evidence of the structure. Although the spectrum was recorded using air-sensitive techniques and was reproduced, the value of the spectra was deemed low when using it for characterization.

Unfortunately, the solid dark red crystals when removed from the glove box show a change in color and decomposition to air. This prognosis was confirmed when dissolved **1** in pyridine and observed through UV-vis spectra, showed significant spectral changes within minutes of exposing the volume to air. The exposed Pb^{+2} ions are likely oxidized by ambient oxygen creating lead-oxo complexes, providing rationale for the complex's sensitivity.

As stated in the introduction, one measure of propellant effectiveness is the heat of combustion (ΔH_c) of the substance, so calorimetry experimentation was conducted to evaluate the ΔH_c of **1**.

Complex **1** mean ΔH_c was -7,012.5 cal/g, 16.5% increase over the stand-alone ligand (-6014.5 cal/g) (Figure 14).[4]

Figure 13. Bomb calorimetry data for **1**

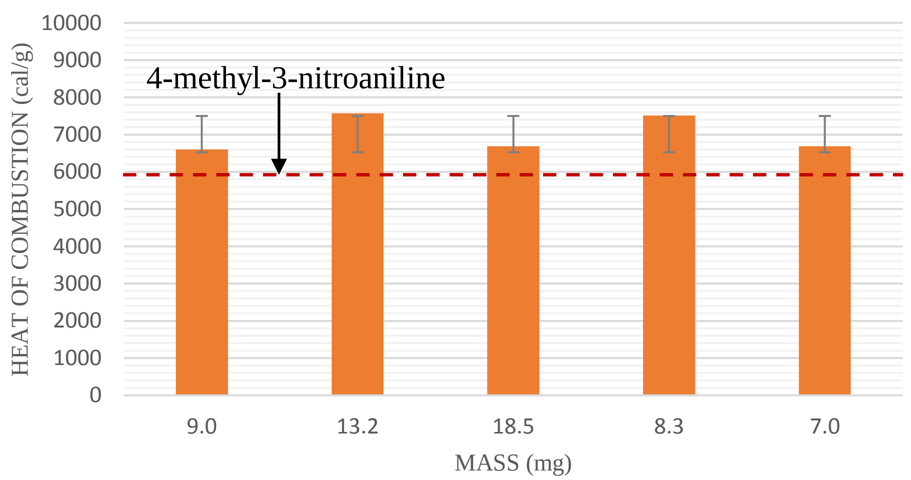

This ΔH_c is significantly higher than that of NC (-1606 cal/g).[5]

A measurement not yet discussed, but significant, is the energy density of a complex. The calculation of energy density of **1** assumes a density equivalent to that of the crystal structure, 2.526 g/cm3. This high density is the possible result of interaction between nitro groups and adjacent Pb atoms, and from hydrogen bonding between adjacent methyl groups. This high density coupled with modest ΔH_c increase with the added lead ions, produces a mean energy density of 74.1 MJ/L for complex **1**.

Figure 15 shows that the combustion energy density is more than three times that of the nitroamine-based high explosives and the high density of the compound is the clear driver for the unexpected results. It is possible that the energy density reported is actually lower than the true value due to the various THF solvate within the molecule. Drying over 24-48 hours by vacuum reduced an amount of THF molecules per crystal, but it is unclear if further removal of THF would increase or decrease the heat of combustion. It should be noted also that **1** has a low oxygen balance (-71% for formation of CO2, -40% for formation of CO), meaning external oxygen is

Figure 14. Energy densities of nitroamines and **1**

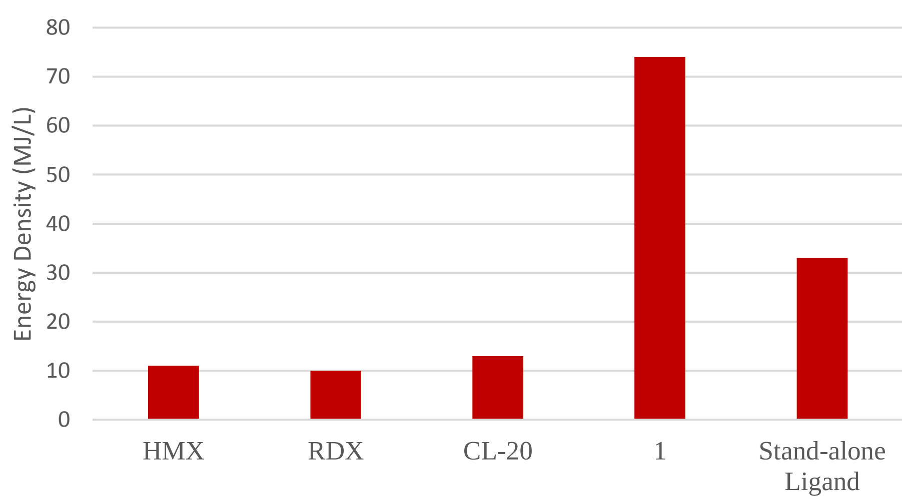

required to complete combustion of this complex. **1** releases 16% more cal/g than the ligand so the oxidation of the added metal increases heat of combustion as expected.

3.2.2 Bis(dinitrophenyl imido lead(II))

A reaction of lead bis(trimethylsilyl)amide with NDPA produced a second novel crystal **2**. For charge balance, two equivalents of NDPA was used for the reaction, and the reaction is illustrated below in Equation 6.

$$Pb[(N(Si(CH_3)_3)_2)] + 2[(C_6H_5)_2(NH_2)(NO_2)] \xrightarrow[23°C,\ 48\ hrs]{THF}$$

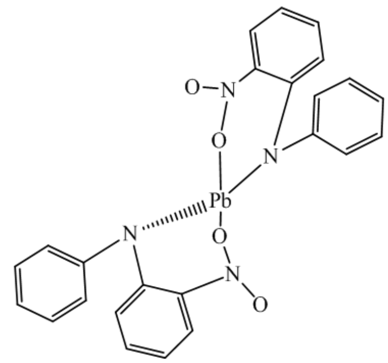

Bis(dinitrophenyl lead(II))

(Equation 6)

The dark purple crystal complex Bis(dinitrophenyl imido lead(II)) is a monoclinic system with the spacegroup of $P2_1/n$. There is one Pb^{+2} cation with two attached nitrodiphenyl ligands in the asymmetric unit. A thermal ellipsoid plot generated is shown below (Figure 17).

The asymmetric unit has a seesaw geometry with 161.4° between oxygen atoms and the obtuse angle between nitrogen atoms is 82.7°. The Pb-N bonds are 2.36 Å, while Pb-O bonds are 2.42 Å. The **2** Bravais lattice is primitive as in **1** but is less aggregated, than in **1**. The exposed Pb^{+2} atom forms a pi-stack with neighboring molecule.

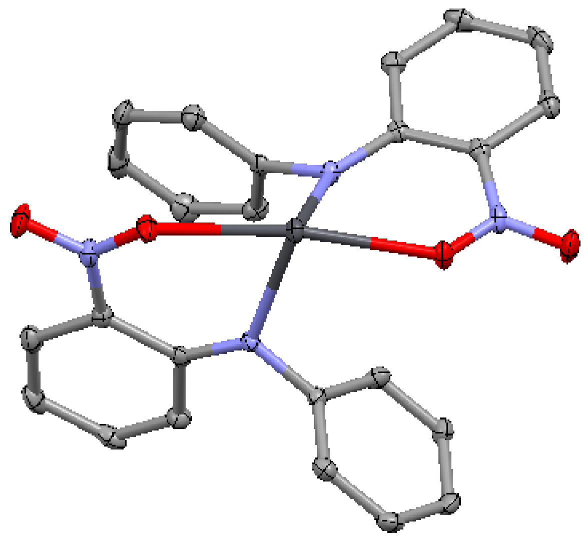

Figure 15. Thermal ellipsoid plots of **2**. Ellipsoids set at 50% probability level, hydrogens and THF solvate omitted for clarity.

Different solvents were attempted to dissolve **2,** with only benzene being capable at room temperature within a few minutes. **2** was not soluble in THF, ACN, HMDS, pyridine, toluene, pentane or ethanol. However, using deuterated benzene produced ^{1}H NMR spectra that supports the proposed structure and is found below in Figure 16.

CHN analysis supported the structure with one co-crystalized THF molecule within the lattice. Drying the molecule removed some THF but 5 THF were left in the crystal for approximately every 9 lead complex of **2**. Theoretical %CHN was calculated for $C_{24}H_{20}N_4O_4$ Pb · 0.55 $(CH_2)_4O$: C, 46.69%; H, 3.3%; N, 8.32%, and found C, 45.57%; H, 3.192%; N, 7.99%.

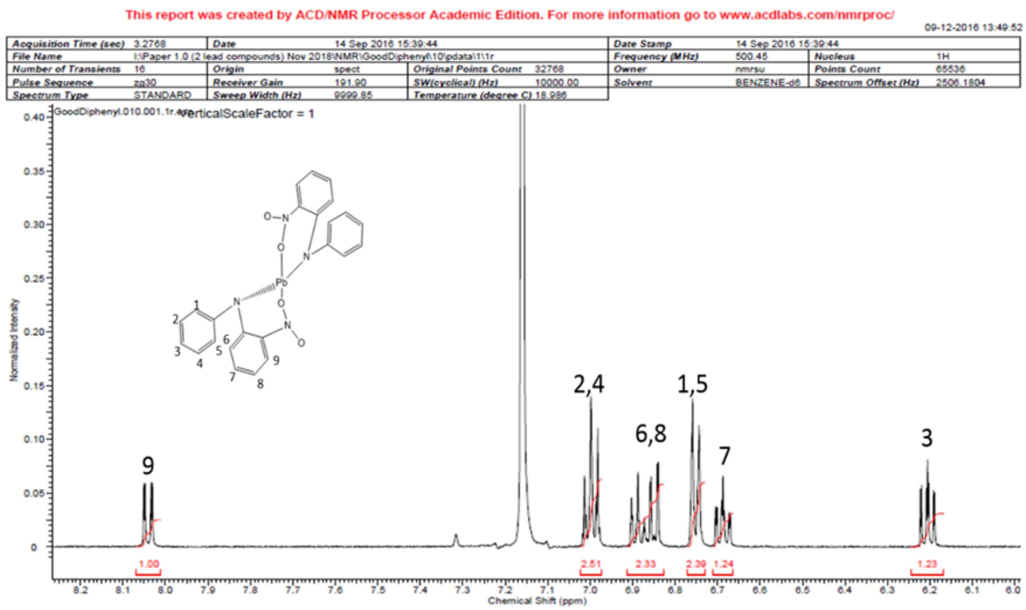

Figure 16. ^{1}H NMR spectra of 2

The IR spectrum for crystal **2** provides more supporting evidence of the chemical structure than observed with **1** (Figure 19). There is a weak signal observed around 3000 cm^{-1} for C-H aromatic stretching although signals at 1250 cm^{-1} and 1100 cm^{-1} indicate a substituted benzene aromatic. A strong signal at the 1500 cm^{-1} supports the presence of a nitroso compound, also found in complex **2**.

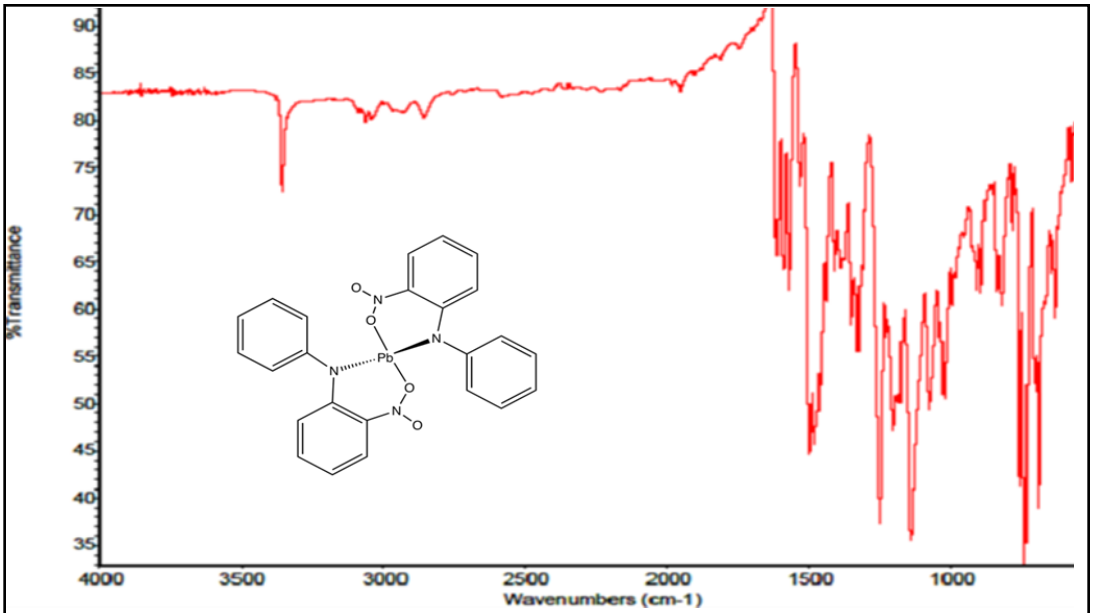

Figure 17. FTIR spectra of **2**

As with complex **1**, the ΔH_c for **2** was determined using a bomb calorimeter. However, complex **2** mean ΔH_c was -4893.2 cal/g, 29.5% below the NDPA ligand (-6947.8 cal/g) (Figure 18).[5]

Figure 18. Bomb calorimetry data for **2**

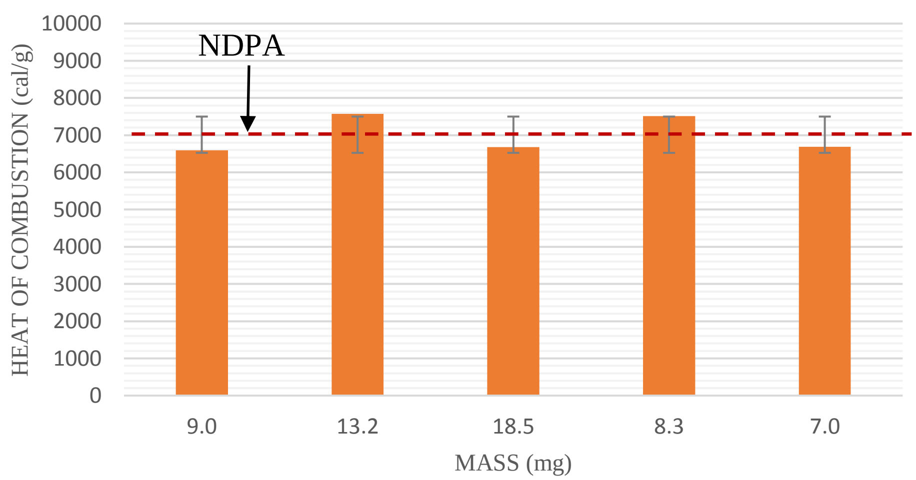

Complex **2** energy density was 38.2 MJ/L. Significant when compared to other nitroamines, but possesses lower crystal density of 1.869g/cm3 compared to **1** (Figure 19). The oxygen balance was low (-136% for formation of CO_2, -75% for formation of CO). Unlike **1**, the heat of combustion was lower of the product then the stand-alone ligands so oxidation of the lead did not show similar combustion results.

Figure 19. Energy densities of nitroamines and complex **2**

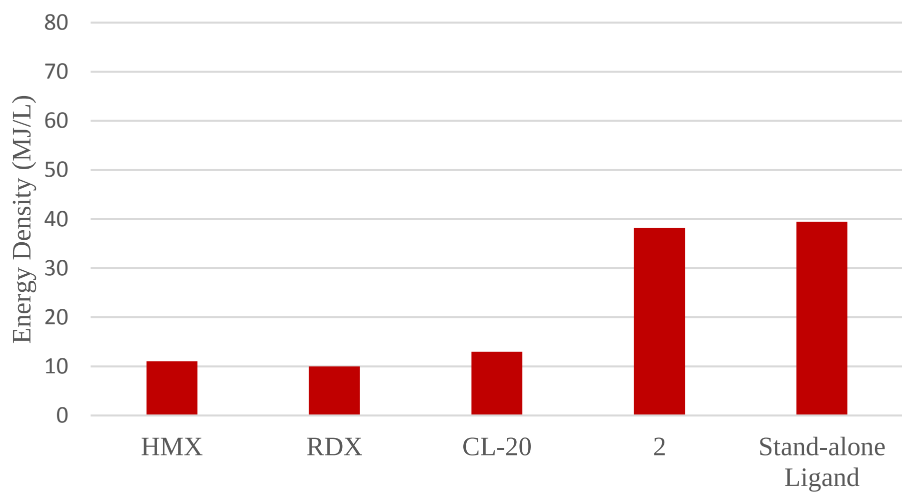

Neither complex displayed shock or friction sensitivity under rudimentary tests, but were highly air-sensitive making burn rate testing impossible. Determination if **1** or **2** modified DB propellant desirably was not accomplished. Unfortunately, other metal and stabilizer reactions were observed but none crystallized and showed poor ability for characterization using a variety of tools.

3.3 References

1. Fjeldberg, T.; Hope, H.; Lappert, M.F.;, Power, P.P.; Thorne, A.J. Molecular Structures of the Main Group 4 Metal(ii) Bis(trimethylsily1)-amides $M[N(SiMe_3)_2]_2$ in the Crystal (X-Ray) and Vapour (Gas-phase Electron Diffraction), *J. Chem. Soc. Chem. Comm.,* **1983,** 639-641.

2. Bürger, H.; Sawodny, W.; Wannagat, U. Darstellung und schwinkungsspektren von silylamiden der elemente zink, cadmium und quecksilber. *J. Organomet*. Chem. 3 **1965**, (2): 113–120.

3. Vehkamäki, M.; Hatanpää, T.; Ritala, M.; Leskelä, Ma. Bismuth precursors for atomic layer deposition of bismuth-containing oxide films. *Journal of Materials Chemistry*. **2004**, 14, 21, 3191.

4. Sullivan, M.V.; Hunt, H., Heats of combustion. IV. The heats of combustion of five aromatic amines, *J. Phys. Chem*., **1949**, 53, 497-500.

5. Cox, J.D.; Pilcher, G., *Thermochemistry of Organic and Organometallic Compounds*, Academic Press, New York, 1970, 1-636.

CHAPTER 4

CONCLUSION

4.1 Summary of Results

Of the 36 reactions using various metals and two different stabilizers under different reaction temperatures and various crystallization techniques only complexes **1** and **2** discussed earlier were crystalized successfully. Many results using various metals ended in amorphous solids that appeared to be crystalline in structure until tested using XRD. In fact, color changes were observed and solids formed in every case, indicating that a reaction took place in each of the 36 attempts, but the products could not be well characterized.

The two crystals produced were both highly sensitive to air, making any burn rate experiments infeasible. Air sensitivity should have been anticipated given the reactants. Nevertheless, it was not anticipated, and prevented experimentation that would have helped answered the research question. However, some questions related to the thesis question were answered: (1) it was demonstrated that $Pb(N(SiMe_3)_2)$ reacted with two types of double-base propellant stabilizer and can readily form crystalline structures, (2) non-lead metal bis(trimethyl)amides do not readily crystalize with the propellant stabilizers mentioned in this manuscript, and (3) organometallic complexes formed using the reactants described produce air-sensitive products. The air-sensitivity of the products prevented answering the thesis question. Therefore, the question whether lead or other metals can be combined with propellant stabilizer to form a better propellant additive remains unanswered.

4.2 Unexpected High Energy Density Lead Species

The formation of tetrakis(μ_3-(4-methyl-3-nitrophenyl imido lead (II))) (**1**) yielded a novel energy dense cubane molecule that exhibits an energy density far greater than traditional nitroamine explosives, commonly used in many military applications. It was surprising that adding a mild energetic ion as lead(II) unexpectedly added energy to the molecule. This energy was probably a result of both the oxidation of Pb(II) to Pb(IV) (forming Pb(IV)O_2 during combustion), and from the increase in density from clustering. The combustion of the material does not produce all low weight gases, thereby decreasing the number of moles in the ideal gas law. The low oxygen balance would also likely result in a slow combustion reaction. However, it is feasible that given the higher heat of combustion and denser material, the lower number of moles produced might be offset and an increase pressure observed, not otherwise expected from an organometallic complex combustion. The distinctive structure of **1** with the energy density make it a complex for future study.

4.3 Future Research

At the time of writing this manuscript, efforts are underway to add capping ligands to complex **1** to make it air-stable and thereby provide an opportunity to test energy density in an authentic aerobic environment. Once stable enough for burn rate testing, the complex could be tested to determine if **1** both demonstrates desirable burn rate characteristics and adequately stabilizes the propellant. Further ligand scaffolding could be used to increase the oxygen balance of the molecule increasing its utility. The molecule shows promise within the energetics field and worthy of modification and future study.

Unfortunately, using the same reaction mechanism for lead did not work for other similar metals in producing crystalline compounds. Copper was not used as a reactant and should also be explored in future research. Additionally, using titanium and zirconium also could be worthy of future examination due to their behavior as highly reducing fuels. However, not only were tin, bismuth, and zinc complexes not identified, but they too would likely be air-sensitive weakening the usefulness of the reactions. Only two propellant stabilizers were used as potential ligands – additional stabilizers, should be explored with various metals in pursuit of both propellant additive and in energetic compound formation. Study could be done to help explain why lead so readily formed well characterized products whereas other similar metals did not. We anticipate future efforts using this methodology may still yield the desired end results, but additional reaction steps and/or adjustment to reactants are required if crystallizing novel desirable double-base propellant additives is to be a success.

CHAPTER 5

EXPERIMENTAL

5.1 Experimental Details

Lead bis(trimethylsilyl)amide and synthesized lead compounds are air sensitive. Therefore, all reactions and experiments were conducted in dry, anaerobic conditions using a glovebox and utilizing air sensitive techniques. All reagents were purchased from Sigma-Aldrich. The solvents used were purified by distillation from sodiumbenzophenone ketyl. Solvents were degassed and stored over molecular sieves for 12h before use. X-ray crystal structure determinations were performed using Bruker Kappa APEX II DUO diffractometer equipped with an Oxford Cryostream. Mo Kα radiation was used for single-crystal structural determination. The crystals were mounted on MiTeGen loops using Paratone-N oil. Data collection, including strategy, unit cell refinement, integration, scaling, and absorption correction was performed using the Bruker APEX2 suite (Bruker, 2008). Space group determination was performed using XPREP (Sheldrick). The ^{1}H NMR spectra were obtained on a Bruker Biospin AVANCE 400MHz spectrometer. CHN analysis were performed by the CENTC elemental analysis facility at the University of Rochester (NY). FT-IR spectra was collected from a Thermo Scientific IR with iD5 ATR and the UV-vis spectra was obtained on a Shimadzu UV-1800.

5.2. Synthesis of Reactants

5.2.1 Lead bis(trimethylsilyl)amide

A lead bis(trimethylsilyl)amide reactant was made using an analogous metathesis reaction to a previously described procedure by Andersen et al.[1] 12.107g of PbI_2 (461.01 g/mol, 25.26 mmol) was dissolved in ~200 mL of THF. 9.817g of $K(N(SiMe_3)_2)$ was dissolved in ~100mL of THF and added drop wise to the PbI_2. After stirring for 12 hours at room temperature the contents were dried under vacuum for 24 hours. Pentane was added to the solid product and filtered through a medium frit. The light-yellow filtrate was and stored at -30°C. Crystals formed and were decanted and rinsed in pentane after 48 hours in storage. The yield produced approximately 6g of lead bis(trimethlysilyl)amide (11.36 mmol, 47%). The resulting structure was indexed and characterized using X-ray diffraction with Mo Kα radiation, unit cell (XRD) orthorhombic P, a = 13.15(3), b = 15.58(3), c = 21.92(5), α = 90.0°, β = 90.0°, γ = 90.0°.

5.2.2 Tin bis(trimethylsilyl)amide

Tin lead bis(trimethylsilyl)amide was available commercially but was back ordered, so it was synthesized using an analogous metathesis reaction to the previously described procedure. 4.2g of $SnBr_2$ (278.518 g/mol, 15.0 mmol) was dissolved in ~100 mL of THF. 3.0g (14.9 mmol) of $K(N(SiMe_3)_2)$ was dissolved in ~100mL of THF and added drop wise to the $SnBr_2$. After stirring for 12 hours at room temperature the contents were dried under vacuum for 24 hours. Pentane was added to the solid product and filtered through a medium frit. The collected light orange filtrate was stored at -30°C. Crystals formed and were decanted and washed in pentane after 48 hours in storage. The yield produced approximately 3.34g of tin bis(trimethlysilyl)amide (10.77 mmol, 31%).

5.2.3 Bismuth bis(trimethylsilyl)amide

A lead bis(trimethylsilyl)amide reactant was made using an analogous metathesis reaction based on a previously described procedure.[1] 3.0g of BiI_3 (589.69 g/mol, 5.01 mmol) was dissolved in ~200 mL of THF. 1.0g (5.0 mmol) of $K(N(SiMe_3)_2)$ was dissolved in ~100mL of THF and added drop wise to the BiI_3. After stirring for 12 hours the contents were dried under vacuum for 24 hours. Pentane was added to the solid product and filtered through a medium frit filter. The light-yellow filtrate was stored at -30 ℃. Powder formed and was decanted, washed in pentane and then dried by vacuum. Produced 1.59g of bismuth bis(trimethlysilyl)amide (2.69 mmol, 47%). The resulting structure melting point was recoded using a warm oil bath and stir bar, the observed range was near reported literature range of 133℃ and 137℃.

5.2.5 Zinc bis(trimethylsilyl)amide

A Zinc bis(trimethylsilyl)amide reactant was made using an analogous metathesis reaction based on a previously described procedure above.[1] 11.10g of $ZnBr_2$ (225.20.01 g/mol, 49.29 mmol) was dissolved in ~200 mL of THF. 9.832g of $K(N(SiMe_3)_2)$ was dissolved in ~100mL of THF and added drop wise to the $ZnBr_2$. After stirring for 12 hours at room temperature the contents were dried under vacuum for 24 hours. Pentane was added to the solid product and filtered through a medium frit. The colorless filtrate was stored at -30°C. A white cloudy solid formed and was collected after 48 hours in storage. The yield produced approximately 5.49g of zinc bis(trimethlysilyl)amide (11.36 mmol, 47%). The synthesized product matched literature melting point range of 12.5 ℃.

5.3 Synthesis of Primary Products

Except where otherwise noted, all operations were carried out under rigorous exclusion of air and water, as compound **1,** and compound **2** are air sensitive.

5.3.1 Tetrakis(μ_3-4-methyl-3-nitrophenylamido)lead (II) (1)

To 66 mg (152.1g/mol, 0.43 mmol) of nitromethylaniline in 2mL of THF was added 144 mg (527.9g/mol, 0.28 mmol) lead bis(trimethylsilyl)amine in 2mL of THF at room temperature giving a color change to dark orange. This solution was then placed in a vapor diffusion double-vial apparatus with the reaction mixture in an inner vial and pentane in the outer vial and left at room temperature. Dark orange crystals were observed 24 hours later. The crystals were subsequently washed 3-5 times with 3mL aliquots of pentane and dried in vacuo. X-ray diffraction was used to characterize the crystal as a tetrakis complex **1**. Unit Cell (XRD): a = 10.4265(16)Å b = 13.2813(19)Å c = 14.624(2)Å, α = 97.592(3)°, β = 94.084(4)°, γ = 99.410(3)°. V = 2068.6(4) Å^3 (Appendix A). Yield: 56mg (0.0373 mmols, 56%). Anal. Calcd for $C_{28}H_{24}N_8O_8Pb_4 \cdot 1 (CH_2)_4O$: C, 25.60%; H, 2.15%; N, 7.46%. Found: C, 25.44%; H, 1.99%; N, 7.41%. UV-Vis pyridine: 391 max [nm] Ɛ = 1.4×10^4 (Appendix B). ^{1}H NMR (C_5D_5N, ppm, 293k): δ8.58 (m, pyridine), δ7.44 (m,pyridine), δ7.06 (m, pyridine), δ6.88 (s,1H), δ5.93 (m,1H) δ 4.84 (m, 1H) δ 2.23 (m, Me) .

5.3.2 Bis(dinitrophenylamido)lead (II) (2)

To 264 mg (527.9 g/mol, 0.5 mmol) of lead bis(trimethylsilyl)amide in 2mL of THF was added 2 equivalents, 214 mg (214.2g/mol, 1.0 mmol) of 2-nitrodiphenylamide in 2mL of THF at room temperature to give a dark purple color. A vapor diffusion double-vial apparatus was used with pentane in the outer vial and reaction mixture in the inner vial and stored at room temperature for 4 days. Purple crystals were formed. The mothor liquor was decanted and the crystals were subsequently washed 3-5 times with 3 mL pentane and dried under vacuum. X-ray diffraction characterized the crystals as bis(dinitrophenylamidolead(II)). Unit Cell (XRD) a = 11.7362 (14), b = 10.8203 (13), c = 20.5003 (2), α = 90.0°, β = 104.766(2)°, γ = 90.0°. V = 2514.6(5) Å^3 (Appendix C). Yield: 264 mg (.0373 mmols, 42%). Anal. Calcd for $C_{24}H_{20}N_4O_4$ Pb · 0.55 $(CH_2)_4O$: C, 46.69%; H, 3.3%; N, 8.32%. Found: C, 45.57%; H, 3.192%; N, 7.99%. UV-Vis benzene: 427 max [nm] Ɛ = 8.9x10^3 (Appendix D).).^{1}H NMR (C_6D_6, ppm, 293k): δ7.93 (m, 1H), δ7.06 (s, C_6D_6), δ6.78 (t, 1H), δ6.77 (m, 1H), δ6.65 (d,1H) δ6.59 (m, 1H), δ6.11 (m, 1H). FT-IR spectra was produced.

5.4 Calorimetry

Calorimetry experiments were conducted using a 6725 semimicro calorimeter attached to a 6772 calorimic thermometer from Parr Instruments. The combustion reactor was a 1109X oxygen combustion vessel and pressurized with O_2 to 35 atm. Pellets of each compound were made by use of a Parr pellet press, and five were made of each product weighing between 5mg and 227mg. Each pellet was trapped between two adhesive plastic strips in an anaerobic glovebox to prevent exposure to air prior to combustion initiation, and transferred to the combustion vessel. When determining the internal energies of the lead compounds, the mean specific heat of the plastic strips was determined to be 5,952.33 cal/g and subtracted from gross heat produced. This modified procedure for air sensitive testing was evaluated using the accepted value of -6318.4 cal/g for benzoic acid and plastic strips. The ΔH_c percent error was determined to be higher by 0.86%. For experimental measurements on **1** and **2**, heats of combustion in cal/g were converted to MJ/L using the experimental crystallographic densities of **1** and **2**.

5.5 References

1. Andersen, R.A.; Faegri, K.; Green, J.; Haaland, A.; Lappert, M. F.; Leung, W.P.; Rypdal, K. *Inorg. Chem.* **1988**, 27, 1782.

2. Fjeldberg, T.; Hope, H.; Lappert, M.F.;, Power, P.P.; Thorne, A.J. Molecular Structures of the Main Group 4 Metal(ii) Bis(trimethylsily1)-amides $M[N(SiMe_3)_2]_2$ in the Crystal (X-Ray) and Vapour (Gas-phase Electron Diffraction), *J. Chem. Soc. Chem. Comm.*, **1983,** 639-641.

BIBLIOGRAPHY

Andersen, R.A.; Faegri, K.; Green, J.; Haaland, A.; Lappert, M. F.; Leung, W.P.; Rypdal, K. *Inorg. Chem.* **1988**, 27, 1782.

Apatoff, J. B.; Norwitz, G. *Role of Diphenylamine as a stabilizer in propellants; analytical chemistry of diphenylamine in propellants*; US Army Armament Command, Test Report T73-12-1, 1973.

A. T. Camp, Patent US 3,088,858, 1963.

Ballistic Modifier LC-12-15 Mil Spec, courtesy of parchem, www.parchem.com/Ballistic-Modifier-LC-12-15-Mil-Spec-getpdf-013001.aspx (accessed 15 March 2017).

Bhat, V.K.; Singh, H. Cross-Linked Slurry Cast Composite Modified Double Base Propellants: Mechanical Properties. *Def Sci J.*, **1987**, 37,1, 39-44.

Braeunig, Robert A., Rocket and Space technology, http://www.braeunig.us/space/propuls.htm (accessed 5 January 2017).

Bürger, H.; Sawodny, W.; Wannagat, U. Darstellung und schwinkungsspektren von silylamiden der elemente zink, cadmium und quecksilber. J. Organomet. Chem. 3 1965, (2): 113–120.

Composition of Type N5 Nitrocellulose-based Double Base Propellant, courtesy of Island Pyrochemical Industries, http://www.islandpyrochemical.com/military/rocket_propellants.php, (accessed 10 December 2016).

Cox, J.D.; Pilcher, G. Thermochemistry of Organic and Organometallic Compounds, Academic Press, New York, 1970, 1-636.

Denisyuk, A.P.; Demidova, L.A. Effect of Some Catalysts on Combustion of Double-Base Propellants, *Combustion, Explosion, and Shock Waves, **2004**, 40, 3 311-318.*

Fifer, R.A. *Workshop Report: Fundamental Reactions in Solid Propellant Combustion;* ARBRL-TR-02166; 1979.

Fjeldberg, T.; Hope, H.; Lappert, M.F.; Power, P.P.; Thorne, A.J. Molecular Structures of the Main Group 4 Metal(ii) Bis(trimethylsily1)-amides $M[N(SiMe_3)_2]_2$ in the Crystal (X-Ray) and Vapour (Gas-phase Electron Diffraction), *J. Chem. Soc. Chem. Comm.*, **1983,** 639-641.

Gao, J.; Wang, L.; Yu, H.; Xiao, A.; Ding, W. Recent Research Progress in Burning Rate Catalysts. *Propellants, Explos. Pyrotech*. **2011**, 36, 404 – 409.

Hamilton, C.R.; Gau, M. R.; Baglia, R. A.; Mc Williams, S. F.; Zdilla, M. J.; Mechanistic Elucidation of the Stepwise Formation of a Tetranuclear Manganese Pinned Butterfly Cluster via N-N Bond Cleavage, Hydrogen Atom Transfer, and Cluster Rearrangement, *Journal of the American Chemical Society*, **2014**, 136, 17974-17986.

Kubota, N. *Propellants and Explosives*, WILEY-VCH Verlag GmbH & Co. KGaA, Weinheim, 2007.

Magill, B. T.; Nauflett, G. W.; Furrow, K. W. *Lead-Free Double-Base Propellant for the 2.75 Inch Rocket Motor;* 20000116525; Cocoa Beach, FL, 2000.

Otto, K.;Lehman, C.;Bartosiewicz, L.;Shelef, M. *Carbon*. **1982**, 20, 243-251.

Raman, K.V., Singh, H., Ballistic Modification of RDX-Based CMDB Propellants, *Propellants Explos. Pyrotech*., **1988**, 13*, 5, 149-151*.

Ramnarace, J. *Rocket Propellant Technology*, Page publishing: New York, NY, 2015.

Sharma, J., Wilmot, G.B., Campolattaro, A.A., Santiago, F., XPS Study of Condensed Phase Combustion in Double-Base Rocker Propellant with and without Lead Salt-Burning Rate Modifier*, Combustion and Flame, **1991**, 85, 416-426.*

Sullivan, M.V.; Hunt, H., Heats of combustion. IV. The heats of combustion of five aromatic amines, *J. Phys. Chem*., **1949**, 53, 497-500.

Tunestål, E.; Hafstrand, A.; Lindborg, A.; Krumlinde, P.; Ek, S.; Goede, P.; Schragen, C. New stabilizers for NC-propellants Evaluated in Rocket Propellants. FOI, Swedish Defense Research Agency, Department of Energetic Materials and Modelling, SE-147 25 Tumba, Sweden.

Vehkamäki, M.; Hatanpää, T.; Ritala, M.; Leskelä, Ma. Bismuth precursors for atomic layer deposition of bismuth-containing oxide films. Journal of Materials Chemistry. 2004, 14, 21, 3191.

Wang, C.; Li, J.; Fan, X.; Zhao, F.; Zhang, W.; Zhang, G.; Gao, Z.; 5-Ferrocenyl-1H-tetrazole-Derived Transition-Metal Complexes; Synthesis, Crystal Structures and Catalytic Effects on the Thermal Decomposition of the Main Components of Solid Propellants, *Eur. J. Inorg. Chem.*, **2015**, 1012-1021.

Yang, V. Thakre, P. Encyclopedia of Aerospace Engineering, Blockley, R. and Shyy, W., Ed; John Wiley and Sons, Ltd: **2010**.

Zain-ul-Abdin, L.W.; Yu, H.; Saleem, M.; Abbasi, N.;Ullah Khan, R.; Ullah, R. S.; Haroon, Mu. Synthesis of ferrocene-based saccharides and their anti-migration and burning rate catalytic properties. *RSC Adv.*, **2016**, 6, 97469–97481.

APPENDIX A

CRYSTAL DATA FOR

TETRAKIS (μ_3-(4-METHYL-3-NITROPHENYL IMIDO LEAD (II)))

Table 1 Crystal data and structure refinement for tetrakis(u3-(4-methyl-3-nitrophenyl imido (II))).

Identification code	tetrakis(u3-(4-methyl-3-nitrophenyl imido (II)))
Empirical formula	$C_{36}H_{40}N_8O_{10}Pb_4$
Formula weight	1573.52
Temperature/K	99.89
Crystal system	triclinic
Space group	P-1
a/Å	10.6519(13)
b/Å	13.5498(16)
c/Å	14.8146(17)
α/°	97.453(2)
β/°	95.652(2)
γ/°	100.455(2)
Volume/Å^3	2068.6(4)
Z	2
ρ_{calc}g/cm^3	2.526
μ/mm^{-1}	16.294
F(000)	1440.0
Crystal size/mm^3	0.159 × 0.099 × 0.022
Radiation	MoKα (λ = 0.71073)
2Θ range for data collection/°	3.092 to 56.022
Index ranges	$-14 \le h \le 13$, $-14 \le k \le 17$, $-17 \le l \le 19$
Reflections collected	24435
Independent reflections	9852 [R_{int} = 0.0308, R_{sigma} = 0.0395]
Data/restraints/parameters	9852/40/527
Goodness-of-fit on F^2	1.056
Final R indexes [I>=2σ (I)]	R_1 = 0.0246, wR_2 = 0.0629
Final R indexes [all data]	R_1 = 0.0315, wR_2 = 0.0655
Largest diff. peak/hole / e Å^{-3}	1.88/-1.15

Table 2 Fractional Atomic Coordinates (×10^4) and Equivalent Isotropic Displacement Parameters (Å^2×10^3) for tetrakis(u$_3$-(4-methyl-3-nitrophenyl imido lead (II))). U$_{eq}$ is defined as 1/3 of of the trace of the orthogonalised U$_{IJ}$ tensor.

Atom	*x*	*y*	*z*	U(eq)
Pb1	4062.6(2)	8475.9(2)	2230.2(2)	13.27(5)
Pb2	2240.7(2)	6137.1(2)	2609.2(2)	14.27(5)
Pb3	4453.1(2)	6170.9(2)	983.9(2)	13.76(5)
Pb4	5589.5(2)	6791.1(2)	3366.4(2)	13.63(5)
O4	10272(4)	7400(3)	2794(3)	29.3(9)
O9	7171(4)	5459(3)	2593(3)	28.7(9)
O6	5091(4)	2344(3)	677(3)	27.8(9)
O5	3600(4)	1227(3)	1068(3)	30.6(10)
O2	-2365(4)	6759(3)	-40(3)	28.7(10)
N7	4299(4)	2078(3)	1190(3)	20.4(10)
O8	3611(4)	10870(3)	6345(3)	25.2(9)
O1	-1797(4)	5369(3)	-532(3)	34.2(11)
O3	11357(4)	8857(3)	2609(3)	31(1)
N8	3313(5)	10422(4)	5556(3)	23.7(10)
N1	2786(4)	6984(3)	1416(3)	14.9(9)
O7	3067(6)	10867(4)	4917(3)	57.8(17)
N3	4132(4)	5565(3)	2335(3)	16.5(9)
C16	3863(5)	4247(4)	3334(4)	20.2(11)
N6	10339(4)	8231(4)	2527(3)	20.5(10)
C5	-203(5)	6815(4)	-151(3)	16.3(11)
C27	3476(5)	8957(4)	4500(3)	16(1)
N5	-1551(4)	6267(3)	-244(3)	18.4(9)
C25	3070(5)	8736(4)	6073(3)	19.5(11)
C26	3274(5)	9327(4)	5379(3)	16.7(11)
C11	9235(5)	9154(4)	1466(4)	19.4(11)
C6	620(5)	6636(4)	579(3)	14.3(10)
C20	4271(5)	3812(4)	1799(4)	16(1)
C18	3919(5)	2496(4)	2792(4)	18.2(11)
C4	149(5)	7436(4)	-787(3)	18.4(11)
C13	8019(5)	7910(4)	2274(3)	15.7(10)
C15	4093(5)	4561(4)	2476(3)	13.9(10)
C22	3500(4)	7939(4)	4244(3)	11.2(9)
C9	6898(5)	8707(4)	1211(3)	16(1)
C19	4161(5)	2820(4)	1968(3)	15.6(10)
N2	5663(4)	7504(3)	2056(3)	14.1(9)
C12	9166(5)	8462(4)	2075(3)	16.0(11)
C8	6837(5)	8032(4)	1857(3)	15.1(10)

C2	2273(5)	7791(4)	78(3)	17.5(11)
C23	3287(5)	7332(4)	4937(4)	20.5(11)
C14	10454(5)	9779(4)	1235(4)	24.2(12)
C7	-765(6)	7559(5)	-1580(4)	26.9(13)
C17	3811(5)	3270(4)	3484(4)	21.4(12)
C10	8053(5)	9244(4)	1027(3)	17.1(11)
C3	1425(5)	7925(4)	-648(3)	17.9(11)
C24	3079(6)	7716(4)	5802(4)	23.5(12)
C29	7523(6)	5319(5)	1684(4)	25.3(12)
C30	8423(6)	4583(5)	1682(4)	28.5(13)
N4	3720(4)	7526(3)	3377(3)	14.7(9)
C28	2789(6)	9102(4)	7023(4)	26.4(13)
C21	3797(6)	1428(4)	2986(4)	26.1(13)
C1	1913(5)	7136(4)	704(3)	14.8(10)
C32	7426(7)	4621(5)	3040(4)	36.1(16)
C31	7890(6)	3903(5)	2338(4)	31.0(14)
O10	9593(14)	7978(12)	4918(9)	210(6)
C35	9921(13)	7246(11)	6204(8)	119(5)
C36	9500(14)	8126(12)	5881(10)	134(5)
C33	9260(20)	6763(14)	4722(12)	199(9)
C34	9388(17)	6212(11)	5542(11)	155(6)

Table 3 Anisotropic Displacement Parameters (Å^2×10^3) for tetrakis(u$_3$-(4-methyl-3-nitrophenyl imido lead (II))). The Anisotropic displacement factor exponent takes the form: $-2\pi^2[h^2a^{*2}U_{11}+2hka^*b^*U_{12}+\ldots]$.

Atom	U_{11}	U_{22}	U_{33}	U_{23}	U_{13}	U_{12}
Pb1	13.42(9)	10.91(9)	14.89(9)	-0.91(7)	2.17(7)	2.66(7)
Pb2	13.63(9)	13.04(9)	15.10(9)	-0.14(7)	2.08(7)	1.37(7)
Pb3	15.69(9)	12.51(9)	12.24(9)	-1.75(7)	1.81(7)	3.08(7)
Pb4	14.22(9)	14.12(9)	12.00(9)	-1.28(7)	1.22(7)	3.92(7)
O4	23(2)	32(2)	35(2)	9.3(19)	3.2(17)	9.9(18)
O9	34(2)	30(2)	27(2)	2.1(18)	14.6(18)	16.3(19)
O6	29(2)	24(2)	29(2)	-2.1(18)	12.9(18)	2.4(17)
O5	39(2)	14(2)	33(2)	-2.9(17)	5.0(19)	-2.9(17)
O2	23(2)	34(2)	28(2)	-3.9(19)	6.7(17)	8.3(18)
N7	22(2)	17(2)	22(2)	-1.7(19)	3.9(19)	7.3(19)
O8	26(2)	22(2)	22(2)	-10.9(17)	1.7(16)	1.6(16)
O1	23(2)	16(2)	58(3)	-5(2)	4(2)	-1.0(16)
O3	14.1(19)	34(2)	41(3)	7(2)	-3.1(17)	-2.5(17)

N8	37(3)	17(2)	18(2)	-2.5(19)	10(2)	6(2)
N1	12(2)	15(2)	16(2)	-3.0(17)	1.0(16)	2.3(16)
O7	133(5)	26(3)	23(2)	4(2)	15(3)	37(3)
N3	18(2)	14(2)	17(2)	-1.8(17)	2.8(17)	5.2(17)
C16	21(3)	21(3)	18(3)	1(2)	-1(2)	5(2)
N6	15(2)	26(3)	20(2)	1(2)	3.2(17)	7.4(19)
C5	14(2)	13(2)	18(2)	-6(2)	-1.4(19)	2.1(19)
C27	17(2)	14(2)	16(2)	-0.4(19)	3.9(19)	0.0(19)
N5	19(2)	22(2)	13(2)	0.1(18)	-0.4(17)	4.5(18)
C25	26(3)	16(3)	14(2)	-7(2)	3(2)	1(2)
C26	15(2)	14(3)	19(3)	-6(2)	4.8(19)	2.6(19)
C11	14(2)	22(3)	20(3)	-4(2)	5(2)	2(2)
C6	13(2)	12(2)	17(2)	-1.0(19)	1.4(18)	2.4(19)
C20	13(2)	14(2)	20(3)	0(2)	-0.5(19)	2.6(19)
C18	18(3)	13(2)	23(3)	2(2)	0(2)	4(2)
C4	20(3)	19(3)	16(2)	-1(2)	1(2)	6(2)
C13	19(3)	13(2)	15(2)	-1.0(19)	2.1(19)	5(2)
C15	13(2)	16(2)	13(2)	3.8(19)	0.4(18)	1.1(19)
C22	10(2)	13(2)	9(2)	-3.1(18)	1.0(17)	1.5(18)
C9	18(3)	17(3)	11(2)	-3.5(19)	-2.0(19)	4(2)
C19	12(2)	14(2)	19(3)	-3(2)	2.4(19)	2.0(19)
N2	12(2)	14(2)	15(2)	-3.3(16)	2.5(16)	3.2(16)
C12	12(2)	19(3)	18(2)	-2(2)	2.5(19)	7(2)
C8	17(2)	12(2)	14(2)	-7.5(19)	0.6(19)	4.5(19)
C2	21(3)	15(3)	17(2)	0(2)	5(2)	6(2)
C23	27(3)	14(3)	20(3)	-1(2)	4(2)	6(2)
C14	19(3)	25(3)	27(3)	2(2)	3(2)	2(2)
C7	28(3)	27(3)	24(3)	8(2)	-6(2)	4(2)
C17	27(3)	22(3)	15(3)	4(2)	1(2)	6(2)
C10	18(3)	20(3)	14(2)	2(2)	3.2(19)	5(2)
C3	21(3)	20(3)	14(2)	5(2)	7(2)	4(2)
C24	36(3)	18(3)	19(3)	5(2)	10(2)	5(2)
C29	31(3)	24(3)	23(3)	2(2)	7(2)	10(2)
C30	30(3)	30(3)	29(3)	3(3)	9(2)	11(3)
N4	16(2)	15(2)	13(2)	-3.1(17)	4.9(16)	4.1(17)
C28	41(3)	22(3)	14(3)	-3(2)	9(2)	1(3)
C21	34(3)	18(3)	27(3)	5(2)	2(2)	6(2)
C1	14(2)	14(2)	14(2)	-4.5(19)	1.4(18)	3.7(19)
C32	41(4)	50(4)	26(3)	11(3)	13(3)	23(3)
C31	38(4)	25(3)	36(4)	10(3)	9(3)	15(3)
O10	191(9)	258(10)	175(9)	6(8)	28(7)	51(8)

C35	113(8)	138(9)	106(8)	-2(7)	48(6)	23(7)
C36	105(8)	183(10)	121(9)	40(8)	19(7)	35(7)
C33	200(12)	205(12)	191(12)	43(9)	11(9)	35(9)
C34	169(10)	162(10)	141(10)	28(8)	32(8)	43(8)

Table 4 Bond Lengths for tetrakis(u$_3$-(4-methyl-3-nitrophenyl imido lead (II))).

Atom	Atom	Length/Å	Atom	Atom	Length/Å
Pb1	Pb2	3.5452(4)	C5	C6	1.399(7)
Pb1	Pb3	3.5303(4)	C5	C4	1.377(8)
Pb1	Pb4	3.5349(4)	C27	C26	1.384(7)
Pb1	N1	2.332(4)	C27	C22	1.388(7)
Pb1	N2	2.350(4)	C25	C26	1.394(8)
Pb1	N4	2.279(5)	C25	C24	1.390(7)
Pb2	Pb3	3.5299(4)	C25	C28	1.507(7)
Pb2	Pb4	3.5460(5)	C11	C12	1.380(8)
Pb2	N1	2.295(5)	C11	C14	1.512(8)
Pb2	N3	2.339(4)	C11	C10	1.392(7)
Pb2	N4	2.310(4)	C6	C1	1.403(7)
Pb3	Pb4	3.5565(4)	C20	C15	1.383(7)
Pb3	N1	2.351(4)	C20	C19	1.385(7)
Pb3	N3	2.293(5)	C18	C19	1.381(8)
Pb3	N2	2.335(4)	C18	C17	1.397(7)
Pb4	N3	2.333(4)	C18	C21	1.498(8)
Pb4	N2	2.280(5)	C4	C7	1.497(7)
Pb4	N4	2.383(4)	C4	C3	1.382(7)
O4	N6	1.233(6)	C13	C12	1.391(7)
O9	C29	1.432(7)	C13	C8	1.394(7)
O9	C32	1.440(8)	C22	C23	1.406(7)
O6	N7	1.226(6)	C22	N4	1.393(6)
O5	N7	1.234(6)	C9	C8	1.405(8)
O2	N5	1.223(6)	C9	C10	1.382(7)
N7	C19	1.465(6)	N2	C8	1.402(7)
O8	N8	1.228(5)	C2	C3	1.387(7)
O1	N5	1.208(6)	C2	C1	1.398(8)
O3	N6	1.234(6)	C23	C24	1.373(7)
N8	O7	1.218(7)	C29	C30	1.503(8)
N8	C26	1.466(7)	C30	C31	1.507(9)
N1	C1	1.397(6)	C32	C31	1.511(8)
N3	C15	1.397(7)	O10	C36	1.431(13)

C16	C15	1.421(7)	O10	C33	1.600(15)
C16	C17	1.363(8)	C35	C36	1.468(14)
N6	C12	1.463(6)	C35	C34	1.578(13)
C5	N5	1.476(6)	C33	C34	1.514(15)

Table 5 Bond Angles for tetrakis(u3-(4-methyl-3-nitrophenyl imido lead (II))).

Atom	Atom	Atom	Angle/°	Atom	Atom	Atom	Angle/°
Pb3	Pb1	Pb2	59.852(9)	C15	N3	Pb3	125.3(3)
Pb3	Pb1	Pb4	60.449(9)	C15	N3	Pb4	115.7(3)
Pb4	Pb1	Pb2	60.111(9)	C17	C16	C15	122.4(5)
N1	Pb1	Pb2	39.61(11)	O4	N6	O3	122.6(5)
N1	Pb1	Pb3	41.28(10)	O4	N6	C12	118.1(4)
N1	Pb1	Pb4	83.69(11)	O3	N6	C12	119.3(5)
N1	Pb1	N2	81.08(14)	C6	C5	N5	116.1(5)
N2	Pb1	Pb2	82.53(11)	C4	C5	N5	118.4(4)
N2	Pb1	Pb3	40.94(9)	C4	C5	C6	125.5(5)
N2	Pb1	Pb4	39.50(11)	C26	C27	C22	121.4(5)
N4	Pb1	Pb2	39.73(10)	O2	N5	C5	117.7(4)
N4	Pb1	Pb3	83.82(10)	O1	N5	O2	123.5(5)
N4	Pb1	Pb4	41.79(10)	O1	N5	C5	118.8(4)
N4	Pb1	N1	78.89(15)	C26	C25	C28	125.9(5)
N4	Pb1	N2	80.34(15)	C24	C25	C26	113.4(4)
Pb1	Pb2	Pb4	59.800(7)	C24	C25	C28	120.6(5)
Pb3	Pb2	Pb1	59.865(7)	C27	C26	N8	115.2(5)
Pb3	Pb2	Pb4	60.347(9)	C27	C26	C25	124.5(5)
N1	Pb2	Pb1	40.37(10)	C25	C26	N8	120.4(4)
N1	Pb2	Pb3	41.16(10)	C12	C11	C14	125.9(5)
N1	Pb2	Pb4	83.92(10)	C12	C11	C10	114.9(5)
N1	Pb2	N3	80.17(15)	C10	C11	C14	119.2(5)
N1	Pb2	N4	79.01(15)	C5	C6	C1	118.7(5)
N3	Pb2	Pb1	82.41(11)	C15	C20	C19	120.0(5)
N3	Pb2	Pb3	39.87(11)	C19	C18	C17	114.3(5)
N3	Pb2	Pb4	40.56(10)	C19	C18	C21	125.8(5)
N4	Pb2	Pb1	39.10(11)	C17	C18	C21	119.9(5)
N4	Pb2	Pb3	83.41(10)	C5	C4	C7	122.9(5)
N4	Pb2	Pb4	41.69(10)	C5	C4	C3	114.8(5)
N4	Pb2	N3	81.06(14)	C3	C4	C7	122.3(5)
Pb1	Pb3	Pb4	59.839(6)	C12	C13	C8	120.8(5)
Pb2	Pb3	Pb1	60.283(6)	N3	C15	C16	121.4(4)

Pb2	Pb3	Pb4	60.051(9)	C20	C15	N3	122.7(5)
N1	Pb3	Pb1	40.86(10)	C20	C15	C16	115.8(5)
N1	Pb3	Pb2	39.98(11)	C27	C22	C23	114.8(4)
N1	Pb3	Pb4	82.93(10)	C27	C22	N4	124.0(5)
N3	Pb3	Pb1	83.36(10)	N4	C22	C23	121.2(4)
N3	Pb3	Pb2	40.84(10)	C10	C9	C8	122.2(5)
N3	Pb3	Pb4	40.16(10)	C20	C19	N7	115.5(5)
N3	Pb3	N1	79.96(15)	C18	C19	N7	119.4(5)
N3	Pb3	N2	78.59(15)	C18	C19	C20	125.1(4)
N2	Pb3	Pb1	41.26(10)	Pb3	N2	Pb1	97.80(15)
N2	Pb3	Pb2	83.07(10)	Pb4	N2	Pb1	99.54(15)
N2	Pb3	Pb4	39.03(11)	Pb4	N2	Pb3	100.82(17)
N2	Pb3	N1	80.97(14)	C8	N2	Pb1	115.1(3)
Pb1	Pb4	Pb2	60.089(7)	C8	N2	Pb3	119.7(3)
Pb1	Pb4	Pb3	59.712(7)	C8	N2	Pb4	119.8(3)
Pb2	Pb4	Pb3	59.602(6)	C11	C12	N6	120.5(5)
N3	Pb4	Pb1	82.72(11)	C11	C12	C13	124.0(5)
N3	Pb4	Pb2	40.68(10)	C13	C12	N6	115.4(5)
N3	Pb4	Pb3	39.34(11)	C13	C8	C9	115.6(5)
N3	Pb4	N4	79.67(14)	C13	C8	N2	122.3(5)
N2	Pb4	Pb1	40.96(10)	N2	C8	C9	122.0(4)
N2	Pb4	Pb2	83.43(10)	C3	C2	C1	122.7(5)
N2	Pb4	Pb3	40.16(10)	C24	C23	C22	122.7(5)
N2	Pb4	N3	78.90(15)	C16	C17	C18	122.3(5)
N2	Pb4	N4	79.62(15)	C9	C10	C11	122.5(5)
N4	Pb4	Pb1	39.60(11)	C4	C3	C2	122.0(5)
N4	Pb4	Pb2	40.14(10)	C23	C24	C25	123.2(5)
N4	Pb4	Pb3	81.85(10)	O9	C29	C30	106.4(5)
C29	O9	C32	108.5(4)	C29	C30	C31	101.8(5)
O6	N7	O5	123.1(4)	Pb1	N4	Pb2	101.18(16)
O6	N7	C19	117.9(4)	Pb1	N4	Pb4	98.60(15)
O5	N7	C19	118.9(5)	Pb2	N4	Pb4	98.16(15)
O8	N8	C26	119.0(5)	C22	N4	Pb1	122.5(3)
O7	N8	O8	121.7(5)	C22	N4	Pb2	117.7(3)
O7	N8	C26	119.3(4)	C22	N4	Pb4	114.5(3)
Pb1	N1	Pb3	97.85(15)	N1	C1	C6	121.5(5)
Pb2	N1	Pb1	100.02(15)	N1	C1	C2	122.2(5)
Pb2	N1	Pb3	98.86(17)	C2	C1	C6	116.3(5)
C1	N1	Pb1	114.2(3)	O9	C32	C31	106.8(5)
C1	N1	Pb2	124.9(3)	C30	C31	C32	103.2(5)
C1	N1	Pb3	116.5(3)	C36	O10	C33	99.3(12)

Pb3	N3	Pb2	99.30(17)	C36	C35	C34	114.1(12)
Pb3	N3	Pb4	100.50(17)	O10	C36	C35	104.0(12)
Pb4	N3	Pb2	98.76(15)	C34	C33	O10	117.0(13)
C15	N3	Pb2	113.1(3)	C33	C34	C35	91.4(11)

Table 6 Torsion Angles for tetrakis(u3-(4-methyl-3-nitrophenyl imido lead (II))).

A	B	C	D	Angle/°	A	B	C	D	Angle/°
Pb1	N1	C1	C6	-133.5(4)	C4	C5	C6	C1	1.4(7)
Pb1	N1	C1	C2	46.6(5)	C15	C16	C17	C18	-3.0(8)
Pb1	N2	C8	C13	137.3(4)	C15	C20	C19	N7	176.8(4)
Pb1	N2	C8	C9	-43.8(5)	C15	C20	C19	C18	-2.2(8)
Pb2	N1	C1	C6	-10.4(6)	C22	C27	C26	N8	178.2(4)
Pb2	N1	C1	C2	169.7(3)	C22	C27	C26	C25	-0.5(8)
Pb2	N3	C15	C16	-57.6(5)	C22	C23	C24	C25	-0.6(9)
Pb2	N3	C15	C20	122.3(4)	C19	C20	C15	N3	-177.0(4)
Pb3	N1	C1	C6	113.5(4)	C19	C20	C15	C16	3.0(7)
Pb3	N1	C1	C2	-66.5(5)	C19	C18	C17	C16	3.7(8)
Pb3	N3	C15	C16	-178.8(3)	C12	C11	C10	C9	2.1(7)
Pb3	N3	C15	C20	1.2(7)	C12	C13	C8	C9	2.4(6)
Pb3	N2	C8	C13	-106.6(4)	C12	C13	C8	N2	-178.6(4)
Pb3	N2	C8	C9	72.3(5)	C8	C13	C12	N6	-177.4(4)
Pb4	N3	C15	C16	55.3(5)	C8	C13	C12	C11	-0.2(7)
Pb4	N3	C15	C20	-124.8(4)	C8	C9	C10	C11	0.1(7)
Pb4	N2	C8	C13	18.6(6)	C23	C22	N4	Pb1	179.8(4)
Pb4	N2	C8	C9	-162.5(3)	C23	C22	N4	Pb2	53.3(6)
O4	N6	C12	C11	-155.0(5)	C23	C22	N4	Pb4	-61.2(5)
O4	N6	C12	C13	22.3(6)	C14	C11	C12	N6	-3.6(8)
O9	C29	C30	C31	34.1(6)	C14	C11	C12	C13	179.4(5)
O9	C32	C31	C30	24.5(7)	C14	C11	C10	C9	-179.2(5)
O6	N7	C19	C20	37.3(7)	C7	C4	C3	C2	-178.7(5)
O6	N7	C19	C18	-143.5(5)	C17	C16	C15	N3	179.5(5)
O5	N7	C19	C20	-141.1(5)	C17	C16	C15	C20	-0.5(7)
O5	N7	C19	C18	38.0(7)	C17	C18	C19	N7	179.8(4)
O8	N8	C26	C27	-153.8(5)	C17	C18	C19	C20	-1.2(7)
O8	N8	C26	C25	25.0(7)	C10	C11	C12	N6	175.0(4)
O3	N6	C12	C11	23.4(7)	C10	C11	C12	C13	-2.1(7)
O3	N6	C12	C13	-159.3(5)	C10	C9	C8	C13	-2.4(7)
O7	N8	C26	C27	25.3(8)	C10	C9	C8	N2	178.6(4)
O7	N8	C26	C25	-155.9(6)	C3	C2	C1	N1	178.0(4)

C5	C6	C1	N1	-179.5(4)	C3	C2	C1	C6	-2.0(7)
C5	C6	C1	C2	0.5(7)	C24	C25	C26	N8	-179.1(5)
C5	C4	C3	C2	0.1(7)	C24	C25	C26	C27	-0.4(8)
C27	C22	C23	C24	-0.3(7)	C29	O9	C32	C31	-3.3(7)
C27	C22	N4	Pb1	-0.5(6)	C29	C30	C31	C32	-34.9(6)
C27	C22	N4	Pb2	-127.0(4)	N4	C22	C23	C24	179.4(5)
C27	C22	N4	Pb4	118.5(4)	C28	C25	C26	N8	4.2(8)
N5	C5	C6	C1	-179.9(4)	C28	C25	C26	C27	-177.1(5)
N5	C5	C4	C7	-1.6(7)	C28	C25	C24	C23	177.8(5)
N5	C5	C4	C3	179.7(4)	C21	C18	C19	N7	1.0(8)
C26	C27	C22	C23	0.9(7)	C21	C18	C19	C20	180.0(5)
C26	C27	C22	N4	-178.9(5)	C21	C18	C17	C16	-177.4(5)
C26	C25	C24	C23	1.0(8)	C1	C2	C3	C4	1.8(8)
C6	C5	N5	O2	107.4(5)	C32	O9	C29	C30	-19.5(6)
C6	C5	N5	O1	-74.0(6)	O10	C33	C34	C35	-4(2)
C6	C5	C4	C7	177.1(5)	C36	O10	C33	C34	-18(2)
C6	C5	C4	C3	-1.7(7)	C36	C35	C34	C33	26.4(18)
C4	C5	N5	O2	-73.8(6)	C33	O10	C36	C35	32.1(16)
C4	C5	N5	O1	104.8(6)	C34	C35	C36	O10	-41.5(17)

Table 7 Hydrogen Atom Coordinates (Å×10^4) and Isotropic Displacement Parameters (Å^2×10^3) for tetrakis(u$_3$-(4-methyl-3-nitrophenyl imido lead (II))).

Atom	***x***	***y***	***z***	**U(eq)**
H16	3742	4737	3821	24
H27	3601	9410	4064	19
H6	309	6184	983	17
H20	4469	3978	1219	19
H13	8042	7444	2700	19
H9	6120	8797	890	19
H2	3134	8160	153	21
H23	3288	6628	4801	25
H14A	10899	10238	1784	36
H14B	10238	10177	755	36
H14C	11016	9326	1014	36
H7A	-1251	6891	-1874	40
H7B	-281	7887	-2026	40
H7C	-1362	7980	-1360	40
H17	3696	3109	4079	26
H10	8040	9692	585	21

H3	1730	8366	-1062	21
H24	2933	7262	6235	28
H29A	7954	5973	1526	30
H29B	6750	5042	1233	30
H30A	9320	4934	1904	34
H30B	8391	4198	1062	34
H28A	3580	9498	7387	40
H28B	2462	8517	7318	40
H28C	2141	9529	6981	40
H21A	2905	1067	2811	39
H21B	4044	1434	3642	39
H21C	4364	1083	2631	39
H32A	6634	4274	3253	43
H32B	8093	4864	3576	43
H31A	8566	3589	2628	37
H31B	7172	3360	2023	37
H35A	9640	7180	6814	143
H35B	10873	7370	6280	143
H36A	8604	8143	5997	160
H36B	10067	8767	6189	160
H33A	8370	6548	4413	239
H33B	9836	6535	4285	239
H34A	10016	5757	5502	186
H34B	8553	5846	5680	186

Experimental

Single crystals of $C_{36}H_{40}N_8O_{10}Pb_4$ **[tetrakis(u$_3$-(4-methyl-3-nitrophenyl imido lead(II)))]** were **[]**. A suitable crystal was selected and **[]** on a '**Bruker APEX-II CCD'** diffractometer. The crystal was kept at 99.89 K during data collection. Using Olex2 [1], the structure was solved with the ShelXS [2] structure solution program using Direct Methods and refined with the olex2.refine [3] refinement package using Least Squares minimisation.

1. Dolomanov, O.V., Bourhis, L.J., Gildea, R.J, Howard, J.A.K. & Puschmann, H. (2009), J. Appl. Cryst. 42, 339-341.
2. Sheldrick, G.M. (2008). Acta Cryst. A64, 112-122.
3.

Crystal structure determination of [tetrakis(u$_3$-(4-methyl-3-nitrophenyl imido lead(II)))]

Crystal Data for $C_{36}H_{40}N_8O_{10}Pb_4$ (M =1573.52 g/mol): triclinic, space group P-1 (no. 2), a = 10.6519(13) Å, b = 13.5498(16) Å, c = 14.8146(17) Å, α = 97.453(2)°, β = 95.652(2)°, γ = 100.455(2)°, V = 2068.6(4) Å^3, Z = 2, T = 99.89 K, μ(MoKα) = 16.294 mm^{-1}, $Dcalc$ = 2.526 g/cm^3, 24435 reflections measured (3.092° ≤ 2Θ ≤ 56.022°), 9852 unique (R_{int} = 0.0308, R_{sigma} = 0.0395) which were used in all calculations. The final R_1 was 0.0246 (I > 2σ(I)) and wR_2 was 0.0655 (all data).

Refinement model description

Number of restraints - 40, number of constraints - unknown.

Details:

```
1. Fixed Uiso
 At 1.2 times of:
  All C(H) groups, All C(H,H) groups
 At 1.5 times of:
  All C(H,H,H) groups
2. Restrained distances
 C33-O10 = O10-C36
 1.43 with sigma of 0.02
 C34-C33 = C35-C34 = C36-C35
 1.5 with sigma of 0.02
 C33-C36
 2.33 with sigma of 0.04
 C36-C34
 2.33 with sigma of 0.04
 C33-C35
 2.33 with sigma of 0.04
 O10-C35
 2.36 with sigma of 0.04
 O10-C34
 2.36 with sigma of 0.04
3. Uiso/Uaniso restraints and constraints
Uanis(O10) ≈ Ueq, Uanis(C33) ≈ Ueq, Uanis(C34) ≈ Ueq, Uanis(C35)
≈ Ueq, Uanis(C36) ≈ Ueq: with sigma of 0.01 and sigma for terminal
atoms of 0.015
4.a Secondary CH2 refined with riding coordinates:
 C29(H29A,H29B), C30(H30A,H30B), C32(H32A,H32B), C31(H31A,H31B), C35(H35A,
 H35B), C36(H36A,H36B), C33(H33A,H33B), C34(H34A,H34B)
4.b Aromatic/amide H refined with riding coordinates:
 C16(H16), C27(H27), C6(H6), C20(H20), C13(H13), C9(H9), C2(H2), C23(H23),
 C17(H17), C10(H10), C3(H3), C24(H24)
4.c Idealised Me refined as rotating group:
 C14(H14A,H14B,H14C), C7(H7A,H7B,H7C), C28(H28A,H28B,H28C), C21(H21A,H21B,H21C)
```

This report has been created with Olex2, compiled on 2016.11

APPENDIX B

UV-vis Spectra of

Tetrakis(u$_3$-(4-methyl-3-nitrophenyl imido lead (II)))

Spectrum Peak Pick Report 01/19/2017 01:48:39 PM

Data Set: Pb Tetrakis - RawData

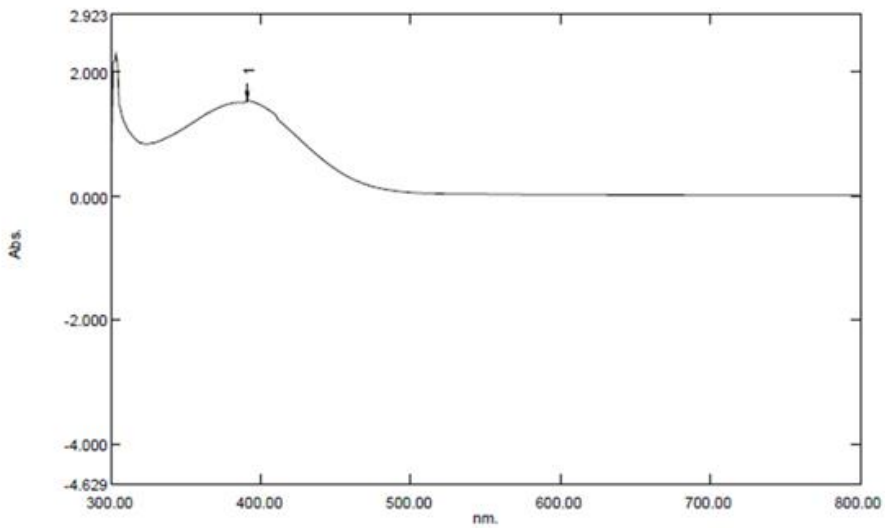

No.	P/V	Wavelength	Abs.	Description
1	P	391.00	1.544	

[Measurement Properties]
Wavelength Range (nm.): 200.00 to 800.00
Scan Speed: Medium
Sampling Interval: 1.0
Auto Sampling Interval: Disabled
Scan Mode: Single

[Instrument Properties]
Instrument Type: UV-1800 Series
Measuring Mode: Absorbance
Slit Width: 1.0 nm
Light Source Change Wavelength: 340.0 nm
S/R Exchange: Normal

APPENDIX C

CRYSTAL DATA FOR

Bis(dinitrophenyl imido lead(II))

Table 1 Crystal data and structure refinement for Bis(dinitrophenyl imido lead(II)).

Identification code	Bis(dinitrophenyl imido lead(II))
Empirical formula	$C_6N_7O_7Pb_6H$
Formula weight	705.76
Temperature/K	100.02
Crystal system	monoclinic
Space group	$P2_1/n$
a/Å	11.7362(14)
b/Å	10.8203(13)
c/Å	20.500(2)
α/°	90
β/°	104.766(2)
γ/°	90
Volume/Å^3	2517.3(5)
Z	4
ρ_{calc}g/cm^3	1.8620
μ/mm^{-1}	6.751
F(000)	1364.1
Crystal size/mm^3	0.095× 0.065 × 0.060
Radiation	Mo Kα (λ = 0.71073)
2Θ range for data collection/°	3.66 to 55.8
Index ranges	$-15 \le h \le 14$, $-11 \le k \le 14$, $-27 \le l \le 20$
Reflections collected	19380
Independent reflections	6006 [R_{int} = 0.0362, R_{sigma} = 0.0376]
Data/restraints/parameters	6006/0/342
Goodness-of-fit on F^2	1.004
Final R indexes [I>=2σ (I)]	R_1 = 0.0265, wR_2 = 0.0699
Final R indexes [all data]	R_1 = 0.0296, wR_2 = 0.0716
Largest diff. peak/hole / e Å^{-3}	3.66/-1.27

Table 2 Fractional Atomic Coordinates (×10^4) and Equivalent Isotropic Displacement Parameters (Å^2×10^3) for mo_3585_0m. U_{eq} is defined as 1/3 of of the trace of the orthogonalised U_{IJ} tensor.

Atom	*x*	*y*	*z*	U(eq)
Pb1	5078.61(10)	7882.25(11)	5111.12(6)	12.82(5)
C6	3735(3)	7296(3)	6376.2(18)	13.1(6)
C50	4259(3)	11871(3)	6586(2)	19.4(7)
C1	3525(3)	7684(3)	7008.3(18)	16.5(7)
C21	10029(3)	7874(4)	6494(2)	21.9(8)
O6	4456(3)	7667(3)	9024.7(16)	29.1(6)
C19	7878(3)	8129(3)	6088.0(16)	12.9(6)
C5	3488(3)	6007(3)	6232.3(17)	14.6(6)
C2	3104(3)	6927(4)	7421.6(19)	20.9(7)
C4	3019(3)	5244(4)	6665.9(19)	20.2(7)
C3	2820(3)	5685(4)	7244.3(19)	22.6(8)
N1	3655(2)	5407(3)	5657.1(15)	16.3(6)
O5	3410(2)	4295(2)	5551.3(14)	25.3(6)
N2	4143(2)	8114(3)	5994.5(14)	12.1(5)
C7	4184(3)	9382(3)	6207.5(16)	13.4(6)
C9	5218(3)	9896(3)	6611.5(17)	16.7(7)
C8	3201(3)	10141(3)	5986.5(17)	15.8(7)
C13	4540(4)	7930(4)	9717(2)	25.7(8)
C12	5801(3)	8348(4)	10004(2)	25.5(8)
C11	6122(3)	8968(4)	9403(2)	28.1(9)
C10	5163(4)	8557(5)	8801(2)	35.8(10)
N3	6804(2)	7653(3)	6026.5(14)	13.0(5)
C23	8120(3)	9347(3)	5875.7(16)	14.9(6)
C20	8917(3)	7426(4)	6410.9(18)	16.7(7)
C22	10230(3)	9071(4)	6276.7(19)	22.9(8)
C15	6519(3)	5441(3)	6184.0(18)	18.2(7)
C16	6337(3)	4471(3)	6591(2)	22.9(8)
C18	6487(3)	5869(4)	7513.3(18)	21.3(7)
C17	6305(3)	4686(4)	7250(2)	24.4(8)
C14	6700(3)	6634(3)	6448.3(16)	13.0(6)
C25	3237(3)	11374(4)	6172.5(18)	19.1(7)
C24	5249(3)	11127(3)	6800.6(18)	18.4(7)
O7	4042(2)	5997(2)	5231.7(13)	18.7(5)
N6	7233(3)	10217(3)	5624.3(14)	15.0(5)
O11	6173(2)	9883(2)	5381.3(12)	16.6(5)
O12	7473(2)	11338(2)	5630.7(15)	25.2(6)
C26	6694(3)	6831(3)	7116.4(18)	17.2(7)

C27	9294(3)	9797(3)	5980.1(18)	18.7(7)

Table 3 Anisotropic Displacement Parameters ($Å^2 \times 10^3$) for mo_3585_0m. The Anisotropic displacement factor exponent takes the form: -$2\pi^2[h^2a^{*2}U_{11}+2hka^*b^*U_{12}+\ldots]$.

Atom	U_{11}	U_{22}	U_{33}	U_{12}	U_{13}	U_{23}
Pb1	14.03(7)	13.13(8)	11.15(8)	-2.86(4)	2.95(5)	0.27(4)
C6	9.8(13)	13.7(16)	15.5(16)	-0.0(11)	2.5(12)	1.6(12)
C50	25.2(18)	11.7(16)	24.0(19)	-0.4(13)	11.1(15)	-2.9(14)
C1	17.2(15)	17.9(17)	14.7(16)	0.1(13)	4.6(13)	-0.2(13)
C21	13.6(16)	33(2)	18.6(18)	4.6(13)	2.2(14)	0.1(14)
O6	25.1(14)	35.0(17)	26.7(15)	-9.9(12)	5.8(12)	-9.2(13)
C19	14.0(14)	14.9(15)	10.0(14)	-1.5(12)	3.1(12)	-0.9(12)
C5	13.9(14)	14.7(16)	14.1(16)	-1.5(12)	1.9(12)	1.7(12)
C2	15.8(16)	33(2)	15.5(17)	1.2(14)	7.3(14)	2.7(15)
C4	19.2(16)	17.2(16)	24.8(18)	-2.6(13)	6.4(14)	5.1(14)
C3	19.2(16)	26(2)	23.7(18)	-2.4(14)	8.3(14)	9.9(15)
N1	17.4(13)	13.6(14)	17.1(14)	-4.7(11)	2.5(11)	-0.0(11)
O5	36.8(15)	10.6(12)	29.0(15)	-8.6(11)	9.3(12)	-2(1)
N2	13.0(12)	12.1(13)	12.0(13)	-1.7(10)	4.7(10)	-0.3(10)
C7	16.0(14)	12.3(15)	13.9(15)	-0.9(12)	7.4(12)	0.3(12)
C9	16.5(15)	15.7(17)	16.8(15)	3.8(12)	2.4(13)	-0.4(13)
C8	13.1(14)	20.9(17)	14.0(15)	-0.3(12)	4.3(12)	1.0(13)
C13	23.8(19)	29(2)	24(2)	-4.8(15)	6.2(17)	-4.2(15)
C12	20.6(17)	26(2)	27(2)	-1.4(15)	1.5(15)	-4.1(16)
C11	23.5(18)	24(2)	38(2)	-4.6(15)	9.5(17)	-4.1(17)
C10	32(2)	49(3)	26(2)	-11(2)	6.6(17)	4(2)
N3	14.6(13)	12.5(13)	11.9(13)	-1.2(10)	3.4(11)	1.6(11)
C23	15.7(14)	17.4(17)	11.5(15)	-2.8(13)	3.7(12)	-0.4(12)
C20	16.6(15)	17.4(17)	16.5(16)	1.5(13)	4.9(13)	0.1(13)
C22	13.5(15)	32(2)	23.8(19)	-7.5(14)	6.5(14)	-3.9(15)
C15	18.9(15)	17.4(17)	18.3(16)	-1.0(13)	4.5(13)	-0.5(13)
C16	24.4(17)	10.7(17)	31(2)	-2.7(13)	2.9(15)	0.5(14)
C18	22.0(17)	26.6(19)	14.9(16)	3.2(14)	3.8(14)	8.1(14)
C17	22.8(17)	19.4(18)	29(2)	-2.1(14)	3.4(15)	12.1(15)
C14	9.9(13)	13.6(16)	14.7(15)	0.5(11)	1.5(12)	2.6(12)
C25	16.5(15)	22.1(18)	21.3(17)	6.6(14)	9.5(13)	3.7(14)
C24	17.6(15)	16.0(17)	21.6(17)	-3.6(13)	5.1(13)	-2.9(13)
O7	23.8(12)	17.3(12)	17.4(12)	-6.7(10)	9.7(10)	-4.1(10)

N6	18.2(14)	14.5(13)	11.9(12)	-5.9(11)	3.3(11)	0.8(10)
O11	14.4(11)	14.2(12)	19.0(12)	-3.2(9)	0.2(9)	4.3(9)
O12	24.6(13)	12.8(12)	35.4(15)	-6.1(10)	2.6(11)	2.6(11)
C26	18.5(15)	16.9(16)	14.9(16)	2.7(13)	1.6(13)	1.1(13)
C27	19.1(16)	20.7(17)	17.8(16)	-7.4(13)	7.2(13)	-1.6(13)

Table 4 Bond Lengths for mo_3585_0m.

Atom	Atom	Length/Å	Atom	Atom	Length/Å
Pb1	N2	2.358(3)	N1	O7	1.255(4)
Pb1	N3	2.397(3)	N2	C7	1.436(4)
Pb1	O7	2.420(2)	C7	C9	1.399(5)
Pb1	O11	2.507(2)	C7	C8	1.394(5)
C6	C1	1.442(5)	C9	C24	1.385(5)
C6	C5	1.440(5)	C8	C25	1.385(5)
C6	N2	1.348(4)	C13	C12	1.516(5)
C50	C25	1.388(5)	C12	C11	1.531(6)
C50	C24	1.390(5)	C11	C10	1.510(6)
C1	C2	1.358(5)	N3	C14	1.426(4)
C21	C20	1.361(5)	C23	N6	1.401(4)
C21	C22	1.410(6)	C23	C27	1.425(5)
O6	C13	1.426(5)	C22	C27	1.361(5)
O6	C10	1.422(5)	C15	C16	1.392(5)
C19	N3	1.338(4)	C15	C14	1.394(5)
C19	C23	1.439(5)	C16	C17	1.380(6)
C19	C20	1.447(5)	C18	C17	1.385(6)
C5	C4	1.423(5)	C18	C26	1.380(5)
C5	N1	1.403(4)	C14	C26	1.388(5)
C2	C3	1.410(6)	N6	O11	1.269(4)
C4	C3	1.352(6)	N6	O12	1.244(4)
N1	O5	1.244(4)			

Table 5 Bond Angles for mo_3585_0m.

Atom	Atom	Atom	Angle/°	Atom	Atom	Atom	Angle/°
N3	Pb1	N2	82.86(10)	C24	C9	C7	120.3(3)
O7	Pb1	N2	70.54(9)	C25	C8	C7	120.9(3)
O7	Pb1	N3	100.32(9)	C12	C13	O6	105.0(3)
O11	Pb1	N2	92.92(9)	C11	C12	C13	103.6(3)

O11	Pb1	N3	68.49(9)	C10	C11	C12	104.1(3)
O11	Pb1	O7	161.51(8)	C11	C10	O6	108.1(3)
C5	C6	C1	113.2(3)	C19	N3	Pb1	128.4(2)
N2	C6	C1	119.9(3)	C14	N3	Pb1	111.65(19)
N2	C6	C5	126.9(3)	C14	N3	C19	117.7(3)
C24	C50	C25	119.4(3)	N6	C23	C19	122.7(3)
C2	C1	C6	123.9(3)	C27	C23	C19	121.7(3)
C22	C21	C20	121.3(3)	C27	C23	N6	115.2(3)
C10	O6	C13	106.7(3)	C19	C20	C21	122.7(3)
C23	C19	N3	125.3(3)	C27	C22	C21	119.4(3)
C20	C19	N3	120.3(3)	C14	C15	C16	119.7(3)
C20	C19	C23	114.3(3)	C17	C16	C15	120.5(4)
C4	C5	C6	121.6(3)	C26	C18	C17	120.0(3)
N1	C5	C6	123.8(3)	C18	C17	C16	119.8(3)
N1	C5	C4	114.6(3)	C15	C14	N3	120.5(3)
C3	C2	C1	120.9(4)	C26	C14	N3	120.1(3)
C3	C4	C5	121.6(4)	C26	C14	C15	119.2(3)
C4	C3	C2	118.7(3)	C8	C25	C50	120.2(3)
O5	N1	C5	121.2(3)	C9	C24	C50	120.6(3)
O7	N1	C5	120.1(3)	N1	O7	Pb1	141.2(2)
O7	N1	O5	118.6(3)	O11	N6	C23	121.1(3)
C6	N2	Pb1	132.8(2)	O12	N6	C23	120.4(3)
C7	N2	Pb1	110.5(2)	O12	N6	O11	118.6(3)
C7	N2	C6	116.1(3)	N6	O11	Pb1	136.8(2)
C9	C7	N2	121.1(3)	C14	C26	C18	120.8(3)
C8	C7	N2	120.2(3)	C22	C27	C23	120.6(3)
C8	C7	C9	118.6(3)				

Table 6 Hydrogen Atom Coordinates (Å×10^4) and Isotropic Displacement Parameters (Å^2×10^3) for mo_3585_0m.

Atom	*x*	*y*	*z*	U(eq)
H50	4281(3)	12712(3)	6721(2)	23.3(8)
H1	3691(3)	8518(3)	7143.9(18)	19.8(8)
H21	10683(3)	7369(4)	6702(2)	26.3(10)
H2	3000(3)	7239(4)	7835.7(19)	25.0(9)
H4	2840(3)	4404(4)	6546.2(19)	24.3(8)
H3	2496(3)	5168(4)	7525.7(19)	27.1(9)
H9	5903(3)	9399(3)	6756.7(17)	20.0(8)
H8	2497(3)	9809(3)	5704.7(17)	19.0(8)

H13a	3980(4)	8591(4)	9760(2)	30.9(10)
H13b	4367(4)	7183(4)	9954(2)	30.9(10)
H12a	5858(3)	8940(4)	10379(2)	30.6(10)
H12b	6324(3)	7635(4)	10169(2)	30.6(10)
H11a	6128(3)	9879(4)	9449(2)	33.7(10)
H11b	6905(3)	8690(4)	9363(2)	33.7(10)
H10a	5516(4)	8189(5)	8455(2)	42.9(12)
H10b	4676(4)	9273(5)	8598(2)	42.9(12)
H20	8820(3)	6620(4)	6571.6(18)	20.1(8)
H22	11012(3)	9369(4)	6336.7(19)	27.5(9)
H15	6521(3)	5292(3)	5727.5(18)	21.9(8)
H16	6233(3)	3655(3)	6415(2)	27.4(9)
H18	6469(3)	6020(4)	7967.1(18)	25.6(9)
H17	6159(3)	4024(4)	7522(2)	29.3(10)
H25	2562(3)	11881(4)	6016.8(18)	23.0(8)
H24	5952(3)	11465(3)	7079.6(18)	22.1(8)
H26	6836(3)	7637(3)	7302.7(18)	20.7(8)
H27	9425(3)	10611(3)	5841.4(18)	22.5(8)

Experimental

Single crystals of $C_6N_7O_7Pb_6H$ **[Bis(dinitrophenyl imido lead(II))]** were **[]**. A suitable crystal was selected and **[]** on a **'Bruker APEX-II CCD'** diffractometer. The crystal was kept at 100.02 K during data collection. Using Olex2 [1], the structure was solved with the ShelXS [2] structure solution program using Direct Methods and refined with the olex2.refine [3] refinement package using Gauss-Newton minimisation.

1. Dolomanov, O.V., Bourhis, L.J., Gildea, R.J, Howard, J.A.K. & Puschmann, H. (2009), J. Appl. Cryst. 42, 339-341.
2. Sheldrick, G.M. (2008). Acta Cryst. A64, 112-122.
3. Bourhis, L.J., Dolomanov, O.V., Gildea, R.J., Howard, J.A.K., Puschmann, H. (2015). Acta Cryst. A71, 59-75.

Crystal structure determination of [Bis(dinitrophenyl imido lead(II))]

Crystal Data for $C_6N_7O_7Pb_6H$ (M =705.76 g/mol): monoclinic, space group $P2_1/n$ (no. 14), a = 11.7362(14) Å, b = 10.8203(13) Å, c = 20.500(2) Å, β = 104.766(2)°, V = 2517.3(5) Å^3, Z = 4, T = 100.02 K, μ(Mo Kα) = 6.751 mm^{-1}, $Dcalc$ = 1.8620 g/cm^3, 19380 reflections measured (3.66° ≤ 2Θ ≤ 55.8°), 6006 unique (R_{int} = 0.0362, R_{sigma} = 0.0376) which were used in all calculations. The final R_1 was 0.0265 (I>=2u(I)) and wR_2 was 0.0716 (all data).

Refinement model description

Number of restraints - 0, number of constraints - 48.

Details:

```
1. Fixed Uiso
 At 1.2 times of:
  All C(H) groups, All C(H,H) groups
2.a Secondary CH2 refined with riding coordinates:
 C13(H13a,H13b), C12(H12a,H12b), C11(H11a,H11b), C10(H10a,H10b)
2.b Aromatic/amide H refined with riding coordinates:
 C50(H50), C1(H1), C21(H21), C2(H2), C4(H4), C3(H3), C9(H9), C8(H8), C20(H20),
 C22(H22), C15(H15), C16(H16), C18(H18), C17(H17), C25(H25), C24(H24),
```

```
C26(H26),
  C27(H27)
```

This report has been created with Olex2, compiled on 2017.01.04 svn.r3372 for OlexSys. Please let us know if there are any errors or if you would like to have additional features.

APPENDIX D

UV-vis Spectra of

Bis(dinitrophenyl imido lead(II))

Spectrum Peak Pick Report

01/25/2017 03:30:10 PM

Data Set: Pb bis - RawData

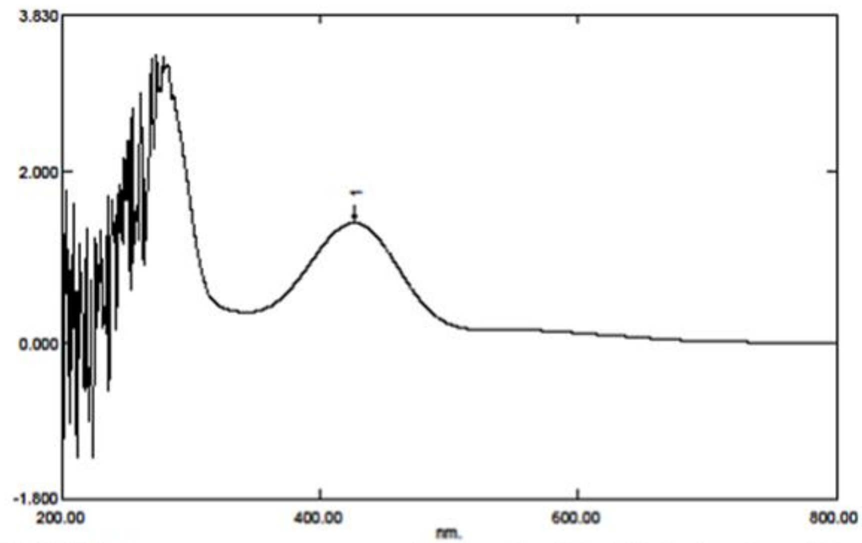

No.	P/V	Wavelength	Abs.	Description
1		427.00	1.398	

[Measurement Properties]
Wavelength Range (nm.): 200.00 to 800.00
Scan Speed: Medium
Sampling Interval: 1.0
Auto Sampling Interval: Disabled
Scan Mode: Single

[Instrument Properties]
Instrument Type: UV-1800 Series
Measuring Mode: Absorbance
Slit Width: 1.0 nm
Light Source Change Wavelength: 340.0 nm
S/R Exchange: Normal